Chapter 6
Macroscopic Fatigue Failure Theories for Multiaxial Stress States

6.1 Introduction

A considerable number of fatigue theories and methodologies for the fatigue life prediction of composite materials and structures have been developed, based on empirical, phenomenological modeling or on the quantification of specific damage metrics, such as the residual strength and/or stiffness of the examined material or structural element. Structural elements made of composite materials were used to be treated as being subjected to uniaxial stress states comprised by the maximum developed stress tensor component, whereas the other components were neglected. This assumption seems reasonable for the highly anisotropic composite materials and was even adopted by the scientific community in the past. For example, a composite wind turbine rotor blade was treated by state-of-the-art design codes, e.g., [1, 2], as a typical beam-like structure for which fatigue life calculations are limited in that they consider only the action of the normal stress component in the beam axis direction. However, regardless of the effect of various model parameters on the accuracy of the theoretical predictions, a strong effect of the transverse normal and shear stress components that develop during service life on the fatigue life has been recorded, e.g., [3]. Theories that do not take into account the interaction of the different stress tensor parameters, like the maximum stress theory (Rankine) or the maximum normal strain theory (Saint Venant) are reliable only for specific cases of isotropic materials e.g. [4], where it is claimed that the maximum stress theory is the most appropriate for isotropic materials that fail due to a brittle fracture, while the maximum shear stress theory or the maximum distortional energy theory seems the most appropriate for the prediction of ductile material behavior. The maximum stress criterion for orthotropic laminae was apparently first suggested in 1920 by Jenkins [5] as an extension of Rankine's theory for isotropic materials. The criterion predicts failure when any principal material axis stress component exceeds the corresponding strength. As shown in [5], since the strengths along the principal material directions provide the input to the criterion, the agreement between the

A. P. Vassilopoulos and T. Keller, *Fatigue of Fiber-reinforced Composites*,
Engineering Materials and Processes, DOI: 10.1007/978-1-84996-181-3_6,

theoretical failure surfaces and the experimental biaxial failure data for a unidirectional graphite/epoxy composite is fair when the applied stress is uniaxial along these directions. However, due to the lack of stress interaction, the accuracy of the predictions is lower in biaxial stress situations.

Nevertheless, quadratic interaction failure criteria that take into account the effect of the different stress tensor parameters on the strength or the fatigue life of the examined materials also exist. One of the first theories of this type was introduced by von Mises, also known as the maximum distortional energy criterion, around 1900 [5]. It is the most widely used quadratic interaction criterion for predicting the onset of yielding in isotropic materials. A generalization of von Mises' theory to incorporate the anisotropic behavior of initially isotropic metals exhibited by the material during large plastic deformations was established by Hill in 1948. This criterion has the drawback that it does not consider the different strength in tension and compression, or even the different positive or negative shear strength that is exhibited by some types of composite materials. One way to take into account the different strength is to include terms which are linear with respect to the normal stresses (to the power of 1) as suggested by Hoffman [6]. This phenomenon, also called *differential failure*, is accommodated by the Tsai-Wu failure criterion introduced in 1971, [7].

It is obvious that a significant number of multiaxial failure theories exist and therefore the selection of the most appropriate one for the examined material and loading conditions is left to the judgment of the design engineer.

The fatigue life prediction is much more complicated since material properties deteriorate during loading. An additional difficulty is caused by the fact that this deterioration is not linear, but depends on the loading conditions and history of loading, i.e., the degree of damage already caused to the material due to previous loading. The inability to simulate material behavior leads to the adoption of high safety factors, which, together with the safety factors due to the stochastic nature of the fatigue phenomenon, result in the overdesign of any structure. New damage-tolerance design philosophies make fatigue theories able to reliably predict the fatigue behavior of a composite material under different loading conditions compulsorily.

Predictive formulations of the fatigue life of composite materials which take stress multiaxiality into account appeared in the 1970s. Most of the proposed criteria were generalizations of static criteria in order to take into account fatigue parameters, such as number of cycles to failure, frequency and stress ratio. Both uniaxial and multiaxial fatigue experiments were performed to assist the development of the fatigue theories and evaluate their predictive ability. Hashin and Rotem [8] proposed a fatigue strength criterion for fiber-reinforced materials based on the different failure modes exhibited. According to the authors, two failure modes exist for unidirectional materials, the fiber and the matrix failure modes. When multidirectional laminates are considered, another failure mode, the interlaminar, is encountered [9]. The Hashin—Rotem failure criterion can be implemented only for materials for which failure modes can be clearly discriminated.

Owen and Griffiths [10] presented a static and fatigue experimental program of glass/polyester thin-walled tubes under combined axial loading and internal pressure in order to evaluate existing multiaxial failure criteria. The authors compared the predictions of the examined failure criteria with the obtained fatigue data and concluded that only those theories that involve complex stress properties provide a reasonable fit. Fujii and Lin [11], in order to validate their experimental, biaxial tension/torsion fatigue data, adapted the Tsai-Wu strength criterion [7] for fatigue. However, the adaptation proved to be insufficient to correctly predict the fatigue behavior of the investigated material system for all the considered fatigue lives. The authors replaced the tensile static strength parameters used in the original version of the Tsai-Wu failure criterion by corresponding S–N curves. However, since they did not have experimental fatigue data under compressive loading they decided to fit the modified Tsai-Wu equation to the available fatigue data for a selected number of cycles in order to estimate the compressive fatigue strength in terms of S–N curves. Therefore, they proved that the proposed form of the Tsai-Wu criterion can accurately model the fatigue behavior of the examined material for certain numbers of cycles–those selected for the fitting of the unknown fatigue strengths – but it fails to predict the behavior for longer fatigue lifetimes.

Sims and Brogdon [12] developed a fatigue failure criterion based on the Tsai-Hill theory. They replaced the static strengths in the Tsai-Hill theory by corresponding fatigue functions. A comprehensive fatigue program comprising a number of tension-tension and interlaminar shear fatigue experiments on S-glass/epoxy and graphite/epoxy unidirectional and cross-ply laminates was performed in order to assist the development of the fatigue theory. Fatigue data on longitudinal, transverse and $\pm 45^\circ$ laminates provided the necessary information to determine the in-plane shear fatigue function, which has been proved significantly different from the interlaminar shear fatigue function. The fatigue strength of any other off-axis laminates can then be obtained through the use of the principal fatigue functions and the established theoretical model. The authors concluded that the proposed theory can be useful for the preliminary fatigue design of fatigue-critical components since it requires limited fatigue data. However, the approach was proved conservative since only the first-ply failure of the examined laminates could be accurately predicted.

Jen and Lee [13, 14] attempted to predict the fatigue behavior of off-axis loaded AS4 carbon/PEEK APC2 unidirectional thermoplastic composite laminates by introducing an appropriately modified version of the Tsai-Hill criterion. They extended the predictive capability of their theoretical formulation for multidirectional laminates made of the same prepreg by means of classical lamination theory (CLT) and ply-discount considerations. Based on the CLT and the assumed ply-discount method for the stiffness degradation of a failed ply, their theoretical predictions for the examined thermoplastic laminates were satisfactorily corroborated by experimental evidence.

An extension of the quadratic version of the Failure Tensor Polynomial, as interpreted by Tsai and Hahn [15], for the prediction of fatigue strength under complex stress states was introduced in [16, 17] by Philippidis and Vassilopoulos.

This strength criterion, established on the basis of the fatigue data presented in Chap. 2, was shown to yield reliable predictions when compared to experimental data from constant amplitude (CA) biaxial fatigue experiments on a wide variety of composite laminates. Satisfactory predictions were also produced using the criterion for the static strength of the GFRP laminate under investigation by testing on- and off-axis specimens in tension and compression. The approach differs from previously mentioned studies, since a direct characterization approach was adopted in [16, 17] for manipulation of the fatigue data and the life prediction of the examined $[0/(\pm 45)_2/0]_T$ laminate. The material was considered a "homogeneous" anisotropic continuum, thus avoiding uncertainties in the modeling of stiffness degradation of failed layers or interlaminar effects and interactions. This is particularly useful for the investigated GFRP laminate, which comprised different glass fabrics with stitched fibers at various orientations. In such cases, simplistic theoretical considerations for load distribution and ply stiffness degradation are no longer applicable.

Kawai [18] examined the off-axis fatigue behavior of unidirectional CFRP composites and developed a fatigue damage mechanics model that could take into account the off-axis angle and stress ratio effect under any constant amplitude loading with non-negative mean stresses. A non-dimensional effective stress parameter was determined by dividing the maximum applied stress at any off-axis angle by the corresponding static strength. The Tsai-Hill criterion was used to calculate static strength at different off-axis angles. The results showed that the model is capable of adequately predicting the off-axis fatigue behavior of unidirectional GFRP and CFPR laminates over a range of non-negative mean stresses.

Fawaz and Ellyin [19] proposed a multiaxial fatigue failure criterion based on only one experimental S–N curve, and the material's static strengths. Multiaxiality is introduced via static failure criteria and S–N curves under complex stress states can be predicted. This criterion constitutes a flexible fatigue failure condition, capable of yielding satisfactory predictions. Wide acceptance is, however, restricted by its high sensitivity to the choice of the single experimental S–N formulation required for its application, as has already been proved elsewhere [17, 20].

The fatigue life prediction of composite laminates has also been addressed from a different perspective, based on the strain energy concept, for the development of a general fatigue failure criterion to take the stress multiaxiality, stress ratio and frequency into account. El Kadi and Ellyin [21] introduced a fatigue failure criterion for unidirectional composite laminates based on the input strain energy that considers both fiber orientation and stress ratio. They found that a normalized form of the criterion can mutate all the fatigue data to fall onto a single line, however, presenting significant scatter. Shokrieh and Taheri [22] developed a fatigue failure model for unidirectional polymer composite laminates based on the static strain energy failure criterion presented in [23]. They also found that use of their theory derives a "master" curve that can adequately model the fatigue behavior of the examined unidirectional material system under any constant amplitude loading pattern.

A review of the multiaxial fatigue theories for composite laminates was recently presented by Quaresimin et al. [20]. As mentioned in [20], although some

of the existing theories are accurate, they cannot always guarantee a safe fatigue design under any loading condition. However, the fairly simple formulation of some of the criteria and their straightforward application make them attractive for design procedures and implementation in numerical codes.

The aforementioned literature review revealed that several methods have been proposed to address the problem of fatigue life prediction of composite materials under multiaxial stress states. A comparison of the predictive ability of the selected methods is presented in this chapter. Fatigue failure theories representative of most of the existing concepts are briefly reviewed and their predictive ability is assessed. The fatigue life prediction performance of the examined fatigue failure criteria will be evaluated on the basis of their capacity to predict the off-axis fatigue behavior of the material system examined in Chap. 2 of this book and other composite material systems from the literature, loaded under uniaxial and biaxial fatigue loads.

6.2 Fatigue Failure Theories

Six multiaxial fatigue failure theories are reviewed in this chapter and their applicability and predicting ability are evaluated. Three of the selected models can be classified as macroscopic fatigue strength criteria, which are usually generalizations of known static failure theories to take into account factors relevant to the fatigue life of the structure such as number of cycles and loading frequency: the Hashin-Rotem (HR) [8], Sims-Brogdon (SB) [12] and the Failure Tensor Polynomial in Fatigue (FTPF) [16, 17]. The applicability of these theories is based on a dataset containing at least three experimentally derived S–N curves, and the static strengths of the material for the HR criterion. Two more macroscopic failure criteria proposed by Kawai (KW) [18] and Fawaz and Ellyin (FE) [19] include the stress ratio in their formulation and can thus be implemented for the prediction of the fatigue life of a composite material for a wide range of loading patterns based on limited databases. The sixth model, introduced by Shokrieh and Taheri (ST) [22], is based on a strain energy concept. The last three criteria are based on one fatigue dataset used for estimation of the model parameters and static strengths of the material that are used in combination with any valid static failure criteria for calculation of off-axis strengths. The S–N curve used is designated “reference” or “master” curve and the methods can be designated “master curve methods”. Other models can be found in the literature as well, but those selected here were proved more accurate, e.g. see [16, 20]. They can be easily implemented, and sufficient fatigue data exist in the literature for evaluation of their accuracy.

6.2.1 Hashin-Rotem

One of the first attempts to generalize a static failure theory in order to take into account factors relevant to fatigue was made by Hashin and Rotem (HR) [8].

The authors presented a fatigue failure criterion based on the different damage modes demonstrated during failure. According to the authors, there are two main modes in the case of unidirectional materials: the fiber failure mode and the matrix failure mode. The discrimination between these two modes is based on the off-axis angle of the reinforcement in relation to the loading direction. The critical fiber angle, which defines the transition from one failure mode to another, is related to the strengths of the material and can be estimated by the following equation:

$$\tan\theta_c = \frac{\tau^s}{\sigma_A^s}\frac{f_\tau(R,N,fr)}{f_A(R,N,fr)} \tag{6.1}$$

where τ^s and σ_A^s are the static shear and longitudinal (axial) strengths, respectively, while the functions $f_\tau(R,N,fr)$, and $f_A(R,N,fr)$ are the fatigue functions of the material along the same directions, and are related to the stress ratio, $R = \sigma_{\min}/\sigma_{\max}$, number of cycles, N and fatigue frequency, fr. The S–N curves of the material under shear, τ, and under longitudinal, σ_A, or transverse, σ_T, directions are given as the product of the static strengths along any direction and the corresponding fatigue function.

If the reinforcement forms an angle of less than θ in relation to the loading direction, the fiber mode is the prevailing failure mode, otherwise the matrix failure mode leads to fatigue failure. Therefore the failure criterion has two forms:

$$\sigma_A = \sigma_A^u \tag{6.2a}$$

$$\left(\frac{\sigma_T}{\sigma_T^u}\right)^2 + \left(\frac{\tau}{\tau^u}\right)^2 = 1 \tag{6.2b}$$

where superscript u denotes fatigue failure stress or the S–N curve of the material in the corresponding direction and subscript T denotes transverse to the fiber direction. It can be shown that any off-axis fatigue function $f''(R,N,fr)$ (matrix failure mode), can be given as a function of, f_τ, f_T, τ^s, σ_T^s and the angle θ [8]:

$$f''(R,N,fr) = f_\tau \sqrt{\frac{1+\left(\frac{\tau^s}{\sigma_T^s}\right)^2\tan^2\theta}{1+\left(\frac{\tau^s}{\sigma_T^s}\frac{f_\tau}{f_T}\right)^2\tan^2\theta}} \tag{6.3}$$

Equation (6.3) can be used not only for the calculation of any off-axis fatigue function, but also to calculate fatigue functions f_τ and f_T, from two different experimentally obtained off-axis fatigue functions. For the application of this criterion over the entire range of on- and off-axis directions, three S–N curves must be defined experimentally, along with the corresponding static strengths of the material.

When the laminate is multidirectional [9], the case is far more complicated. As each lamina is under a different stress field, failure may occur in some laminae after a certain amount of load cycling while the other laminae are still far from

failure. The different stress fields developed in each lamina produce interlaminar stresses, able to cause successive failure. To take these stresses into account, an interlaminar failure mode is established and the set of equations (Eq. 6.2a) is supplemented by:

$$\left(\frac{\sigma_d}{\sigma_d^u}\right)^2 + \left(\frac{\tau_d}{\tau_d^u}\right)^2 = 1 \tag{6.4}$$

where subscript d denotes the interlaminar stress components.

The Hashin and Rotem failure criterion can predict the fatigue behavior of a unidirectional (UD) or multidirectional (MD) laminate subjected to uniaxial or multiaxial cyclic loads provided that the type of failure mode exhibited during fatigue failure can be distinguished. Its use for woven or stitched fabrics is therefore not recommended.

6.2.2 Fawaz-Ellyin

Fawaz and Ellyin (FWE) [19] proposed a fatigue failure criterion to simulate the fatigue behavior of unidirectional and multidirectional composite laminates under multiaxial cyclic stress states. The criterion has the advantage of requiring only one experimentally obtained S–N curve and the static strengths of the laminate along different directions. The idea is based on the assumption that all the on- and off-axis S–N curves of the laminate, when normalized by the corresponding static strengths, lie in a narrow band on the S–N plane. Although this idea had already been proposed in 1981 by Awerbuch and Hahn [24], where a master fatigue curve was demonstrated as being the representative S–N curve of a number of normalized off-axis fatigue datasets, it was Fawaz and Ellyin who developed a failure criterion based on this.

According to this criterion, if a reference S–N curve exists, e.g.,:

$$S_r = m_r log(N) + b_r, \tag{6.5}$$

the S–N curve under any off-axis angle or biaxial ratio can be calculated by:

$$S(a_1, a_2, \theta, R, N) = f(a_1, a_2, \theta)(b_r + g(R)m_r \log(N)) \tag{6.6}$$

as a function of the reference S–N curve.

In Eqs. 6.5 and 6.6, subscript r denotes the reference direction and a_1 and a_2 are the transverse over normal (σ_y/σ_x) and shear over normal (σ_s/σ_x) biaxial stress ratios. Parameters m_r and b_r are derived after fitting to the experimental data, while model functions f and g are non-dimensional and are defined by:

$$f(a_1, a_2, \theta) = \frac{\sigma_x(\alpha_1, \alpha_2, \theta)}{X_r} \tag{6.7}$$

$$g(R) = \frac{\sigma_{\max}(1-R)}{\sigma_{\max_r} - \sigma_{\min_r}} \tag{6.8}$$

with $\sigma_x(a_1, a_2, \theta)$ being the static strength along the longitudinal direction and X_r the static strength along the reference direction. The off-axis static strengths of the examined material can be estimated using any reliable multiaxial static failure criterion, e.g., Tsai-Hahn. As it can be seen from Eq. 6.8, function g is introduced to take into account different stress ratios, R. When the stress ratio of the reference S–N curve is the same as that of the S–N curve being predicted, $g = 1$, while for $R = 1$ (quasi-static loading), g equals 0.

Although the FWE criterion in Eq. 6.5 was initially presented based on the Lin-Log S–N curve representation (following the original formulation as described in [19]), it is obvious that any other type of S–N curve, e.g., Log-Log, can also be used without loss of the generality of the method.

Although the FWE criterion has the advantage of requiring only a minimum amount of data, the predictions are very sensitive to the selection of the reference curve, as it will be shown in the following.

6.2.3 Sims-Brogdon

Sims-Brogdon (SB) [4] modified the Tsai-Hill failure criterion for static strengths to a fatigue criterion by replacing the static strengths with corresponding fatigue functions. As a result, the Tsai-Hill tensor polynomial in fatigue is:

$$\left(\frac{K_1}{\sigma_1}\right)^2 - \frac{K_1 K_2}{\sigma_1^2} + \left(\frac{K_2}{\sigma_2}\right)^2 + \left(\frac{K_{12}}{\sigma_6}\right)^2 = \frac{1}{\sigma_x^2} \tag{6.9}$$

where σ_i, i = 1, 2, 6 denotes the fatigue functions (for the SB criterion the corresponding S–N curves) along the longitudinal, the transverse directions and shear, respectively, and the parameters K_1, K_2 and K_{12} are the ratios of the stresses along the principal material system over the lamina stress in the direction of the load. These parameters are expressions of the cos and sin of the off-axis angle under consideration. The desired laminate fatigue strength at any off-axis angle is designated by σ_x.

This was the first attempt to modify static polynomial failure criteria in order to take fatigue parameters, and especially the number of cycles to failure, into account. However, the criterion refers to lamina fatigue strength and can be extended to laminates of any orientation using laminated plate theory and knowledge of the stresses in the individual lamina to predict first-ply failure. The SB fatigue theory has the same drawback as the Tsai-Hill criterion, which was used as the basis for its development–it does not take the different strengths of the material under tension and compression into account.

6.2.4 Failure Tensor Polynomial in Fatigue

A modification of the quadratic version of the failure tensor polynomial for the prediction of fatigue strength under complex stress states was introduced by Philippidis and Vassilopoulos [16, 17] and designated Failure Tensor Polynomial in Fatigue (FTPF). The theory is based on the Tsai-Hahn tensor polynomial and adapted for fatigue by substituting the failure tensor components with the corresponding S–N curves. Therefore the FTPF criterion can be expressed in the material symmetry axes (1 and 2), under plane stress by:

$$F_{11}\sigma_1^2 + F_{22}\sigma_2^2 + 2F_{12}\sigma_1\sigma_2 + F_1\sigma_1 + F_2\sigma_2 + F_{66}\sigma_6^2 - 1 = 0, \tag{6.10}$$

with the components of the failure tensors given by:

$$F_{11} = \frac{1}{XX'}, F_{22} = \frac{1}{YY'}, F_{66} = \frac{1}{S^2}, F_1 = \frac{1}{X} - \frac{1}{X'}, F_2 = \frac{1}{Y} - \frac{1}{Y'} \tag{6.11}$$

where F_{ii} and F_i are functions of the number of cycles, N, stress ratio, R and the frequency, fr, of the loading since the failure stresses have been substituted with the S–N curves. X, Y and S represent the fatigue strengths of the material (being in general functions of the number of cycles, the stress ratio and the fatigue frequency) along the longitudinal, the transverse directions and under shear loading. The prime′ is used for compressive fatigue strengths. Simple uniaxial constant amplitude fatigue experiments can be used for the derivation of $X(N, R, fr)$ and $Y(R, N, fr)$. However, the application of pure shear stresses on a composite specimen is more difficult. Since methods like the rail-shear test on plane specimens or torsional tests on cylindrical specimens are quite complicated and costly, alternative methods were developed, e.g., [25, 26].

The method for the derivation of the shear fatigue strength as half of the S–N curve of the specimens cut at 45° off-axis was initially examined in [16], for the material systems presented in Chap. 2, and showed satisfactory results for the case of reversed loading. However, as it was proved later, [17], a value of 1/2.2 for the S–N at 45° off-axis offered more accurate results for the reversed loading and the other loading patterns that were examined. An alternative method was also presented in [17] to avoid this inconvenience. According to this, the shear fatigue strength can be estimated directly by means of the FTPF criterion and by the use of one off-axis fatigue curve. This method for the back-calculation of the fatigue shear strength, which is presented in detail later on, has been proved sufficiently accurate, especially for unidirectional composite laminates, without the problems raised by use of the 45° off-axis divided by a factor of 2, or 2.2.

Although the components of the failure tensor presented in Eq. 6.11 can be easily determined by simple uniaxial experiments, the selection of the interactive term, F_{12}, is much more complicated. The burden of biaxial experiments is significant and in several cases the results are not sufficiently reliable, see for example [27 and 28], for a discussion on this subject. Therefore, the selection of

the interactive term is based on experience and geometrical/mathematical considerations:

- The failure locus defined by Eq. 6.10 must include the origin of the co-ordinate system otherwise, the criterion would predict failure even under zero load application.
- It is widely accepted and supported by the experimental evidence that the failure locus must be closed (e.g., ellipse).

The following stability criterion between the failure tensor terms and the interaction term must be met in order to satisfy the aforementioned conditions:

$$F_{11}F_{22} - F_{12}^2 \geq 0 \tag{6.12}$$

or in general:

$$F_{ii}F_{jj} - F_{ij}^2 \geq 0 \tag{6.13}$$

The selection of the form of the interactive term leads to different criteria. The following will be used here:

$$F_{12} = -0.5\sqrt{F_{11}F_{22}} \tag{6.14}$$

although it has been proved, e.g., in [29], that the use of the interaction term in the form:

$$F_{12} = 0.5(F_{33} - F_{11} - F_{22}) \tag{6.15}$$

can provide more accurate predictions. However, the derivation of the out-of-plane strength of the (thin) composite laminates that is required for the application of Eq. 6.15 is a demanding task that outweighs the advantages of the improved predictions, and therefore Eq. 6.14 is preferred.

Substitution of the failure tensor components (Eq. 6.11) and the interaction term (Eq. 6.14) into Eq. 6.10 gives for the plane stress state:

$$\frac{\sigma_1^2}{XX'} + \frac{\sigma_2^2}{YY'} - \frac{\sigma_1\sigma_2}{XY} + \frac{\sigma_6^2}{S^2} - 1 = 0 \tag{6.16}$$

and taking into account the tensorial transformation equations:

$$\begin{aligned} \sigma_1 &= \sigma_x \cos^2\theta \\ \sigma_2 &= \sigma_x \sin^2\theta \\ \sigma_6 &= \sigma_x \sin\theta\cos\theta \end{aligned} \tag{6.17}$$

the fatigue strength (σ_x) at any off-axis angle can be calculated as:

$$\sigma_x = \sqrt{\frac{1}{\left(\frac{\cos^4\theta}{XX'} + \frac{\sin^4\theta}{YY'} - \frac{\cos^2\theta\sin^2\theta}{XY} + \frac{\cos^2\theta\sin^2\theta}{S^2}\right)}} \tag{6.18}$$

Equation 6.18 can also be used for calculation of the S–N curve under shear, when it is not possible to derive it experimentally. For this, an off-axis S–N curve (σ_x) must be used as the reference curve and Eq. 6.18 must be solved for S.

6.2.5 Kawai

Kawai [18] developed a non-dimensional stress parameter-based theory founded on the Tsai-Hill static failure criterion by introducing a non-dimensional effective stress Σ^* that takes the effects of the stress ratio and the state of stress on the fatigue life into account. The non-dimensional effective stress is given by:

$$\Sigma^* = \frac{\frac{1}{2}(1-R)\sigma^*_{\max}}{1-\frac{1}{2}(1+R)\sigma^*_{\max}} \tag{6.19}$$

Equation 6.19 is valid for $|R| \leq 1$. $\sigma^*_{\max}$ is the maximum non-dimensional effective stress which can be calculated by:

$$\sigma^*_{\max} = \Omega(\theta)\sigma_{\max}, \tag{6.20}$$

as a function of the maximum cyclic stress of the developed plane stress state ($\sigma_{\max}(>0)$) and the "orientation factor" [18] given by:

$$\Omega(\theta) = \left(\frac{\cos^4\theta}{X^2} - \frac{\sin^2\theta\cos^2\theta}{X^2} + \frac{\sin^4\theta}{Y^2} + \frac{\sin^2\theta\cos^2\theta}{S^2}\right) \tag{6.21}$$

following the Tsai-Hill failure criterion for quasi-static stress states.The considered fatigue life model is,

$$2N_f = \frac{1}{(\Sigma^*)^{n^*}} \tag{6.22}$$

where $2N_f$ is the number of reversals to failure and n^* is the material constant obtained by fitting to experimental fatigue data. Equation 6.22 shows that the master S–N relationship obtained by plotting the non-dimensional effective stress Σ^* against the number of reversals to failure on logarithmic scales becomes a straight line.

To apply the model for off-axis fatigue simulation, the S–N relationship for each off-axis angle (θ) can be reproduced from the master S–N curve by the following equation:

$$\sigma_{\max} = \frac{2\Sigma^*}{\Omega(\theta)[(1-R)+(1+R)\Sigma^*]} \tag{6.23}$$

Application of the proposed model to the unidirectional glass/epoxy and carbon/epoxy composites under constant amplitude cyclic loading with

non-negative mean stresses [18] showed that the model can adequately describe off-axis fatigue behavior under the examined loading conditions.

6.2.6 Shokrieh-Taheri

Shokrieh and Taheri (ST) [22] proposed a strain energy-based model, derived from the Sandhu static failure energy criterion [23], for predicting the fatigue life of a unidirectional lamina at various fiber angles and stress ratios. They also adopted the assumption of El Kadi and Ellyin [21] that the relationship between fatigue life and total input energy can be described by a power law type equation of the form of Eq. 6.24:

$$\Delta W^t = kN^\alpha + C \tag{6.24}$$

Additionally they assumed $C = 0$ and independency of the fitting parameters, k and α, of the stress ratio and fiber orientation. According to [22] these two parameters can be obtained for each material by using one set of fatigue test data at an arbitrary stress ratio and fiber orientation.

The proposed model, with respect to the on-axis coordinate system, is given by the following equation:

$$\Delta W = \Delta W_I + \Delta W_{II} + \Delta W_{III} = \frac{\Delta\sigma_1\Delta\varepsilon_1}{X\varepsilon_{u1}} + \frac{\Delta\sigma_2\Delta\varepsilon_2}{Y\varepsilon_{u2}} + \frac{\Delta\sigma_6\Delta\varepsilon_6}{S\varepsilon_{u6}} \tag{6.25}$$

where ΔW represents the sum of strain energy densities contributed by all stress components in material directions and Δ before a symbol denotes range, e.g., $\Delta\sigma$ denotes the stress range. W_I, W_{II} and W_{III} denote the strain energy densities in the longitudinal and transverse directions and shear, respectively and can be derived by the set of Eqs. 6.26:

$$\begin{aligned}
\Delta W_I &= \frac{1}{X^2}\frac{(1+R)}{(1-R)}(\Delta\sigma_x)^2\cos^4\theta \\
\Delta W_{II} &= \frac{1}{Y^2}\frac{(1+R)}{(1-R)}(\Delta\sigma_x)^2\sin^4\theta \\
\Delta W_{III} &= \frac{1}{S^2}\frac{(1+R)}{(1-R)}(\Delta\sigma_x)^2\sin^2\theta\cos^2\theta
\end{aligned} \tag{6.26}$$

where, in addition to the material static strengths, X, Y and S, σ_1, σ_2, σ_6, and ε_1, ε_2, ε_6 are stress and strain tensor components, while ε_{u1}, ε_{u2} and ε_{u6} are the maximum strains in the principal material directions.

Assuming a linear stress-strain response along the material directions, the conversion of off-axis stresses into the on-axis coordinate Eq. 6.25 takes the form:

$$\Delta W = \frac{(1+R)}{(1-R)}(\Delta\sigma_x)^2\left(\frac{\cos^4\theta}{X^2}+\frac{\sin^4\theta}{Y^2}+\frac{\sin^2\theta\cos^2\theta}{S^2}\right) \tag{6.27}$$

with θ being the fiber orientation angle. Equation 6.27 is valid as long as $R \geq 0$.

The advantages of this criterion can be summarized in two main points: the criterion uses both stress and strain to predict failure and only one set of data is required (and used as the reference set) for calibration of the model parameters. On the other hand, the model is only applicable to unidirectional laminates. Predictions of the model for glass/epoxy and carbon/epoxy unidirectional laminates were in good agreement with experimental fatigue data in [22].

6.3 Experimental Results from Literature

The described fatigue theories were developed based on experimental data concerning unidirectional and multidirectional composite laminates. Selected data from the literature will be presented in the following paragraphs the demonstration of the application of the fatigue theories and the evaluation of their predictive ability.

All available experimental fatigue data were treated in the same manner. S–N curves of the form:

$$\sigma_a \, or \, \sigma_{\max} = \sigma_o N^{-1/k} \tag{6.28}$$

were fitted to the available databases and used in calculations of fatigue life predictions.

6.3.1 Uniaxial Loading

6.3.1.1 Glass/Epoxy, UD, Flat Specimens (Hashin and Rotem)

A complete set of off-axis fatigue results from unidirectional E-glass/epoxy specimens are presented in [8]. The experiments were performed at three different fatigue frequencies, 34, 19 and 1.8 Hz, and were concluded when the specimen was fractured or when the limit of 10^6 cycles was reached. Tension-tension fatigue loading under the R-ratio of 0.1 was applied. The experimental results for specimens at $\theta = 5°, 10°, 15°, 20°, 30°$ and $60°$ are presented in Figs. 6.1 and 6.2. The parameters for the S–N equations, according to Eq. 6.28, are given in Table 6.1. The S–N curves along the transverse direction (90°) and at 10° were used for calculation of the S–N curve under shear as proposed by the authors [8], using Eq. 6.3.

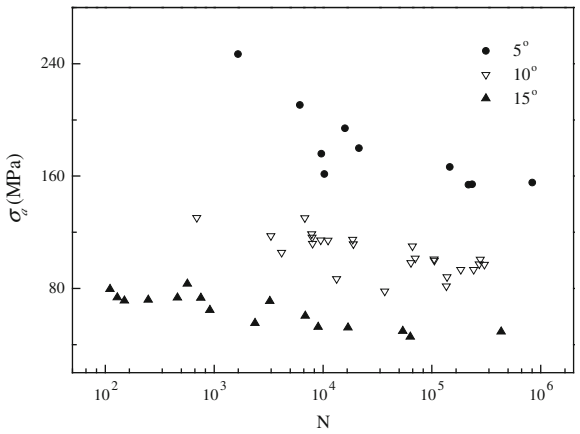

Fig. 6.1 Experimental results Hashin–Rotem [8]. 5°, 10°, 15°, off-axis

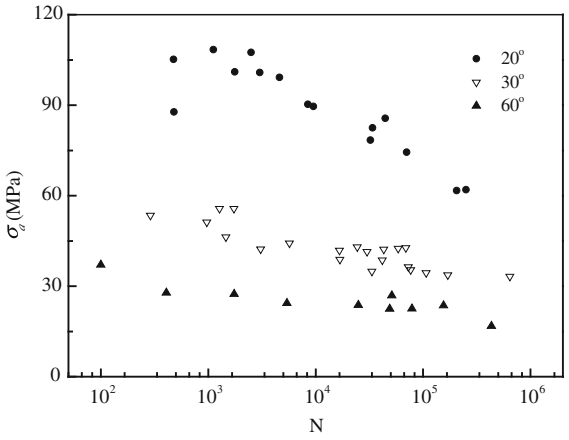

Fig. 6.2 Experimental results, Hashin–Rotem [8]. 20°, 30°, 60°, off-axis

6.3.1.2 Graphite/Epoxy, UD, Flat Specimens (Awerbuch and Hahn)

Awerbuch and Hahn [24] presented the results of an experimental program comprising static and fatigue tests on unidirectional carbon/epoxy specimens.

Constant amplitude loading under $R = 0.1$ at a frequency of 18 Hz was applied until failure or the limit of 10^6 fatigue cycles. The maximum applied cyclic stress was between 50 and 70% of the static strength of the material along each off-axis angle. The experimental results for several on- and off-axis angles are presented in Table 6.2. The off-axis static strengths were calculated using the Tsai-Wu [7] failure criterion and the available static strength data along the principal directions of the examined material. The experimental results from specimens cut at different off-axis angles between 10° and 90° are given in Figs. 6.3 and 6.4.

Table 6.1 S–N curves and corresponding static strengths for experimental data of Hashin–Rotem [8]

Off-axis angle θ	UTS (MPa)	S–N curve (MPa)
0°	1236.09	$\sigma_a = 1740.00N^{-0.0786}$
5°	434.26*	$\sigma_a = 478.65N^{-0.0947}$
10°	216.08*	$\sigma_a = 354.49N^{-0.1186}$
15°	142.98*	$\sigma_a = 221.25N^{-0.1022}$
20°	106.24*	$\sigma_a = 125.24N^{-0.0880}$
30°	69.45*	$\sigma_a = 101.41N^{-0.0913}$
60°	34.81*	$\sigma_a = 56.26N^{-0.0864}$
90°	28.45	$\sigma_a = 41.04N^{-0.0860}$
Shear	37.96*	$\sigma_a = 64.35N^{-0.1118}*$

*value calculated using Eq. 6.3

Table 6.2 S–N curves and corresponding static strengths for experimental data of Awerbuch and Hahn [24]

Off-axis angle θ	UTS (MPa)	UCS (MPa)	S–N curve (MPa)
0°	1836.0	1836.0	$\sigma_{\max} = 1043.29N^{-0.0458}$
10°	458.0		$\sigma_{\max} = 572.77N^{-0.0893}$
20°	211.0		$\sigma_{\max} = 263.75N^{-0.07746}$
30°	129.0		
45°	94.0		$\sigma_{\max} = 168.60N^{-0.1250}$
60°	70.0		$\sigma_{\max} = 80.18N^{-0.0533}$
90°	56.9	207.0	$\sigma_{\max} = 93.61N^{-0.1103}$
Shear	93.0	93.0	

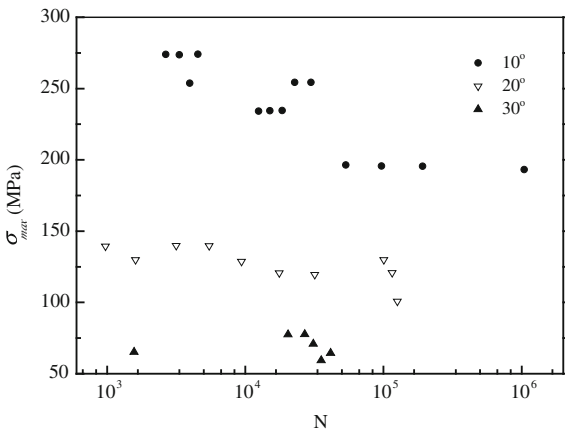

Fig. 6.3 Experimental results, Awerbuch-Hahn [24]. 10°, 20°, 30°, off-axis

As shown in Fig. 6.4, the quality of the off-axis data at high angles is very low. Therefore, only the data from specimens cut at 10°, 20° and 45° off-axis will be used in the next section for evaluation of the fatigue failure criteria.

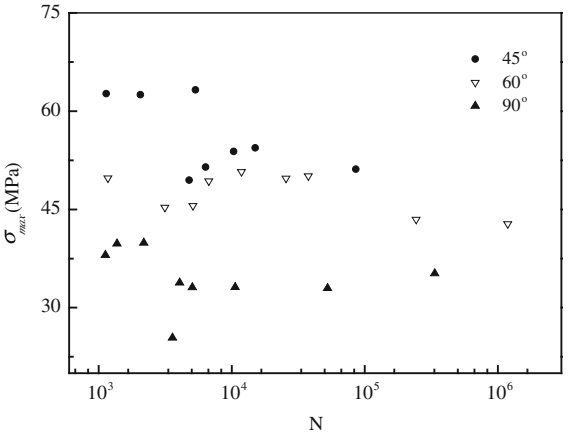

Fig. 6.4 Experimental results, Awerbuch-Hahn [24]. 45°, 60°, 90°, off-axis

6.3.1.3 AS4 Carbon/PEEK APC2, Flat Specimens (Jen-Lee)

The experimental program of Jen and Lee [13, 14] consisted of quasi-static and constant amplitude fatigue tests on unidirectional, cross-ply and pseudo-isotropic laminates. Different *R*-ratios were selected for the fatigue loading, resulting in different applied loading patterns covering both tension-tension and compression-compression fatigue. A constant frequency of 5 Hz was maintained for all studied cases and it was found that Log-Log S–N curves could fit the experimental data accurately. The derived S–N equations for all examined unidirectional specimens are given in Table 6.3. It should be noted that the authors do not provide analytical information regarding the experimental results; they only give the average values of cycles to failure for each stress level, and tabulated information concerning the S–N curve equations corresponding to each loading case.

A modified version of the Tsai-Hill failure criterion proposed by the authors is designated as the "extended Tsai-Hill fatigue failure criterion" (ET-H FFC). Based on this criterion, the authors initially estimated the shear strength of their material by using the experimental data along the directions of 0°, 90° and 45° and then tried to predict material behavior along other off-axis directions.

6.3.2 Biaxial Loading

6.3.2.1 Woven Cylindrical Glass/Polyester Specimens (Owen-Griffiths)

Constant amplitude fatigue data from an experimental program comprising biaxial tests on cylindrical woven, glass/polyester specimens is presented in Owen and Griffiths [10]. An axial load together with internal pressure was applied on the specimens in order to produce the desired biaxial stress states.

Table 6.3 S–N curves for experimental data of Jen and Lee [13, 14]

			S–N curve (MPa)			
θ	UTS (MPa)	UCS (MPa)	$R = 0$	$R = 0.2$	$R=-\infty$	$R = 5$
0°	2 128	955	$\sigma_{max} = 2673.00N^{-0.0503}$	$\sigma_{max} = 2604.47N^{-0.0446}$	$\sigma_{max} = 1235.55N^{-0.0620}$	$\sigma_{max} = 1192.50N^{-0.0548}$
15°	459	461	$\sigma_{max} = 603.67N^{-0.0680}$	$\sigma_{max} = 589.13N^{-0.0630}$	$\sigma_{max} = 608.92N^{-0.0675}$	$\sigma_{max} = 648.78N^{-0.0707}$
30°	221	275	$\sigma_{max} = 287.36N^{-0.0783}$		$\sigma_{max} = 385.23N^{-0.0809}$	
45°	151	228	$\sigma_{max} = 175.54N^{-0.0710}$	$\sigma_{max} = 173.44N^{-0.0622}$	$\sigma_{max} = 277.57N^{-0.0780}$	$\sigma_{max} = 366.51N^{-0.0952}$
60°	116	215	$\sigma_{max} = 158.49N^{-0.0910}$	$\sigma_{max} = 153.70N^{-0.0804}$	$\sigma_{max} = 242.05N^{-0.0677}$	$\sigma_{max} = 338.66N^{-0.0938}$
75°	96	211	$\sigma_{max} = 114.46N^{-0.0782}$		$\sigma_{max} = 206.46N^{-0.0658}$	
90°	93	206	$\sigma_{max} = 116.81N^{-0.0813}$	$\sigma_{max} = 126.80N^{-0.0774}$	$\sigma_{max} = 262.68N^{-0.0879}$	$\sigma_{max} = 274.45N^{-0.0851}$
Shear	133	133				

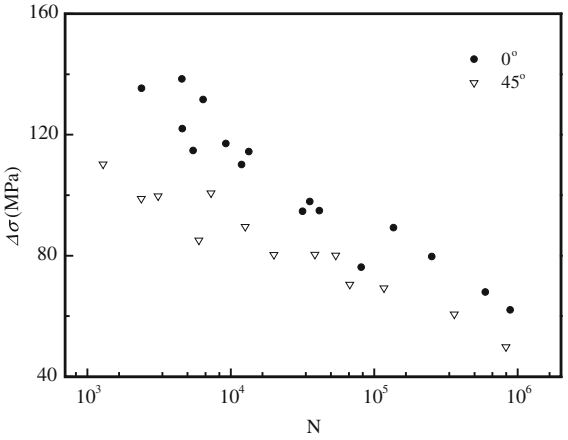

Fig. 6.5 Experimental results, Owen-Griffiths [10]. 0°, 45°

Table 6.4 S–N curves for experimental data of Owen and Griffiths [10]

Angle θ	S–N curve (Mpa)
0°	$\Delta\sigma = 416.75N^{-0.1390}$
45°	$\Delta\sigma = 265.44N^{-0.1183}$

Constant amplitude cyclic loads under a stress ratio, $R = 0$, were applied on the specimens at a constant frequency of 1.8 Hz.

The woven material used exhibited the same properties along the longitudinal and transverse directions. Therefore, only two S–N curves are required (one along the longitudinal/transverse directions and one for shear) for application of the examined fatigue failure criteria.

The authors presented uniaxial experimental data for on-axis and 45° off-axis specimens as shown in Fig. 6.5 as number of cycles to failure under specific values of the stress range. The fitted Log-Log S–N equations are given in Table 6.4. They also performed experiments under five biaxial stress ratios (axial stress over hoop stress) ($a = \sigma_{ax}/\sigma_{hp}$) between –1 and 1 (–1, –0.5, 0, 0.5, 1) in order to simulate the failure loci for different numbers of cycles. The biaxial experimental results are presented in Figs. 6.6 and 6.7 and tabulated in Tables 6.5 and 6.6.

6.3.2.2 Woven Cylindrical Glass/Polyester Specimens (Fujii-Lin)

Another biaxial program was carried out by Fujii and Lin [11]. Cylindrical woven, glass/polyester specimens were tested under biaxial tensile-torsional loading under constant amplitude conditions. A biaxial stress field containing normal and shear stress components developed as a result. The frequency was limited to 2 Hz in order to avoid the development of high temperatures during the application of the loads under an $R = 0$. The uniaxial test results

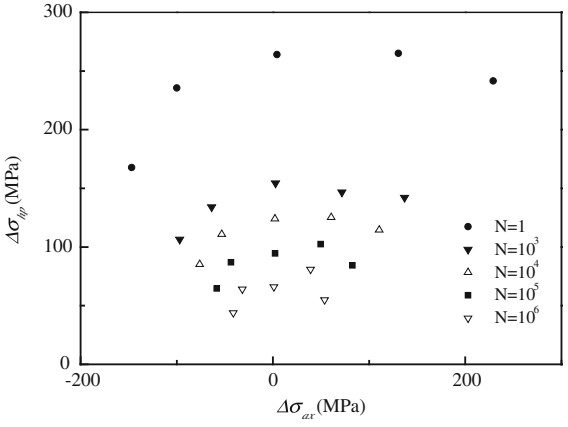

Fig. 6.6 Experimental results, Owen-Griffiths [10]. Failure loci, specimens at 0°

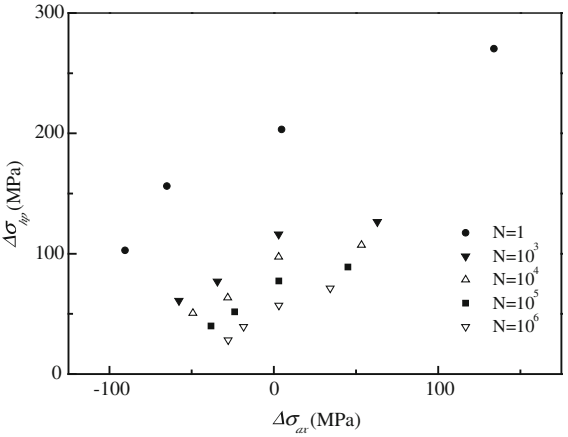

Fig. 6.7 Experimental results Owen-Griffiths [10]. Failure loci, specimens at 45°

Table 6.5 Failure loci for specimens tested at 0°

10^6 cycles		10^5 cycles		10^4 cycles		10^3 cycles		1 cycle	
$\Delta\sigma_{hp}$ (MPa)	$\Delta\sigma_{ax}$ (MPa)	$\Delta\sigma_{hp}$ (MPa)	$\Delta\sigma_{ax}$ (MPa)	$\Delta\sigma_{hp}$ (MPa)	$\Delta\sigma_{ax}$ (MPa)	$\Delta\sigma_{hp}$ (MPa)	$\Delta\sigma_{ax}$ (MPa)	$\Delta\sigma_{hp}$ (MPa)	$\Delta\sigma_{ax}$ (MPa)
55.01	53.67	84.23	82.67	114.49	110.64	142.10	136.96	241.58	229.11
80.92	39.21	102.48	49.74	125.25	60.68	146.60	71.82	265.13	130.42
65.98	1.05	94.49	2.38	124.02	2.07	154.37	2.79	263.93	4.19
64.06	−31.74	86.91	−43.55	110.77	−53.10	134.02	−63.676	235.57	−100.01
43.93	−41.24	64.56	−58.38	85.19	−76.14	106.44	−96.97	167.71	−146.76

Table 6.6 Failure loci for specimens tested at 45°

10^6 cycles		10^5 cycles		10^4 cycles		10^3 cycles		1 cycle	
$\Delta\sigma_{hp}$ (MPa)	$\Delta\sigma_{ax}$ (MPa)	$\Delta\sigma_{hp}$ (MPa)	$\Delta\sigma_{ax}$ (MPa)	$\Delta\sigma_{hp}$ (MPa)	$\Delta\sigma_{ax}$ (MPa)	$\Delta\sigma_{hp}$ (MPa)	$\Delta\sigma_{ax}$ (MPa)	$\Delta\sigma_{hp}$ (MPa)	$\Delta\sigma_{ax}$ (MPa)
71.39	34.27	88.88	45.08	107.19	53.38	126.51	62.94	270.31	133.98
57.12	3.05	77.24	3.01	97.36	2.98	116.06	2.95	203.26	4.70
39.41	−18.39	51.59	−23.82	63.38	−28.01	76.98	−34.28	156.21	−65.02
28.21	−27.75	39.78	−38.18	50.54	−49.24	60.89	−57.80	102.72	−90.57

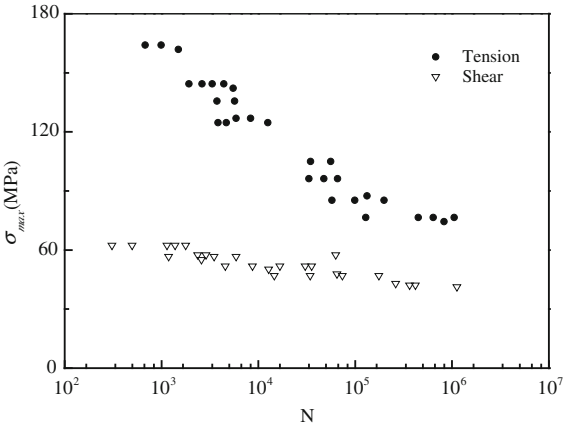

Fig. 6.8 Experimental results, Fujii-Lin [11], tension and shear

Table 6.7 S–N curves for experimental data of Fujii and Lin [11]

Loading pattern	S–N curve (MPa)
Tension	$\sigma_{\max} = 405.65N^{-0.1309}$
Shear	$\sigma_{\max} = 97.05N^{-0.0649}$

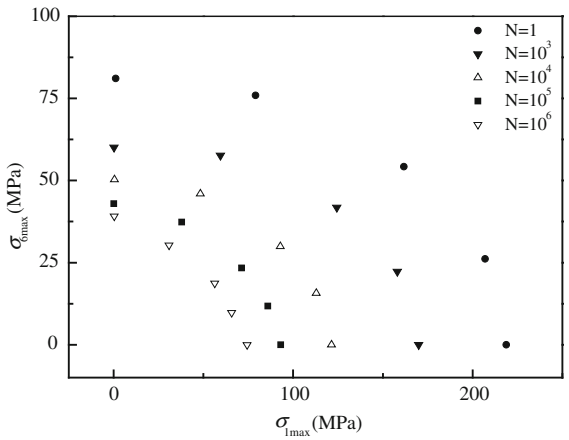

Fig. 6.9 Experimental results, Fujii-Lin [11], failure loci

Table 6.8 Failure loci for specimens tested at 45°

1 cycle		10^3 cycles		10^4 cycles		10^5 cycles		10^6 cycles	
σ_{1max} (MPa)	σ_{6max} (MPa)	σ_{1max} (MPa)	σ_{6max} (MPa)	σ_{1max} (MPa)	σ_{6max} (MPa)	σ_{1max} (MPa)	σ_{6max} (MPa)	σ_{1max} (MPa)	σ_{6max} (MPa)
1.22	81.05	0.23	60.05	0.42	50.25	0.16	42.91	0.30	39.17
79.14	75.89	59.52	57.63	48.29	45.99	37.96	37.31	30.86	30.29
161.77	54.20	124.40	41.76	92.85	29.90	71.25	23.38	56.32	18.74
206.97	26.13	158.03	22.28	112.95	15.69	85.89	11.79	65.77	9.77
218.74	0.00	169.92	0.00	121.4	0.00	93.12	0.00	74.39	0.00

(with biaxial stress ratios $a = \sigma_1/\sigma_6 = 1/0$, tension and $a = 0/1$ shear) are presented in Fig. 6.8, while the fitted Log-Log equations are given in Table 6.7.

Three biaxial stress ratios were obtained in addition to the uniaxial loading cases described earlier. 7/1, 3/1, 1/1, and the experimental results are presented in Fig. 6.9 and tabulated in Table 6.8.

6.4 Fatigue Life Prediction

The fatigue failure theories described under Sect. 6.2 will be used here to predict the fatigue behavior of the composite material systems presented in Chap. 2 and Sect. 6.3. It should be mentioned however that some of the aforementioned criteria, e.g., that proposed by Kawai [18], or that of Shokrieh-Taheri [22], are limited to unidirectional materials and therefore not able to predict the off-axis behavior of the multidirectional composite laminate in Chap. 2, nor the behavior of the woven composites tested under biaxial loading and described in Sect. 6.3. In addition to these, the Hashin-Rotem [8] criterion is not applicable for either multidirectional or woven materials since it is not possible to define whether the dominant failure mode is the fiber or matrix mode.

The Log-Log S–N curve type, e.g., Eq. 6.28, was used in all cases for fitting of the fatigue data for consistency, although the Lin-Log representation was used in the original versions of some of the criteria, e.g., FWE.

6.4.1 Uniaxial Loading

6.4.1.1 Glass/Epoxy, UD, Flat Specimens (Hashin and Rotem)

All examined failure theories were applicable for the estimation of the off-axis fatigue behavior of the material system presented in the paper of Hashin and Rotem [8]. Fatigue functions (S–N curves) of the Log-Log form were used for all theories, when necessary. The comparison of the predictions is presented in

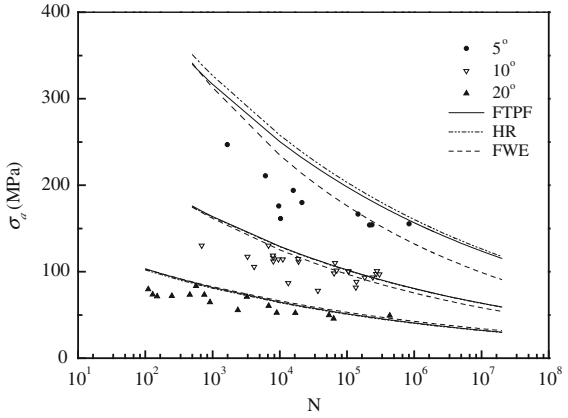

Fig. 6.10 Predicted S–N curves for 5°, 10° and 20° off-axis specimens [8]. FTPF, HR and FWE criteria

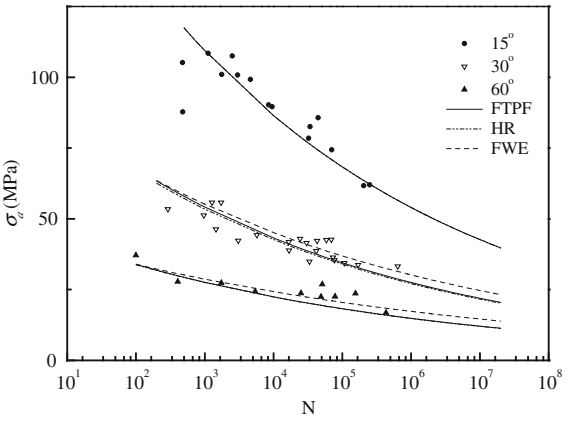

Fig. 6.11 Predicted S–N curves for 15°, 30° and 60° off-axis specimens [8], FTPF, HR and FWE criteria

Figs. 6.10, 6.11, 6.12 and 6.13 for the fatigue data of specimens cut along the off-axis directions between 5° and 60°.

The S–N curve at 15° off-axis was used as the reference curve for the FWE, KW and ST criteria. As shown in Figs. 6.10, 6.11, 6.12 and 6.13, all fatigue theories, except KW, overestimate the fatigue behavior for small off-axis angles (5° and 10°), while they are accurate for the off-axis directions between 15° and 60°. In contrast, KW is more accurate for 5°, 10° and 20°, while it tends to underestimate the material behavior for bigger off-axis angles, e.g., 30° and 60°, see Fig. 6.13. The equations for the predicted S–N curves are given in Table 6.9.

The curves predicted using the HR criterion are the most accurate of the set of plotted curves with $R^2 > 0.86$. FTPF and SB predictions exhibited similar accuracy ($R^2 > 0.82$) although they tend to overestimate the life at the low cycle fatigue regime and be more conservative at the high cycle fatigue regime. FWE, ST and KW produced less accurate predictions.

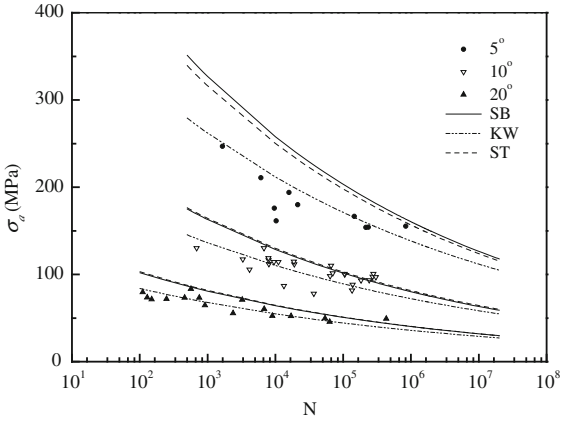

Fig. 6.12 Predicted S–N curves for 5°, 10° and 20° off-axis specimens [8], SB, KW and ST criteria

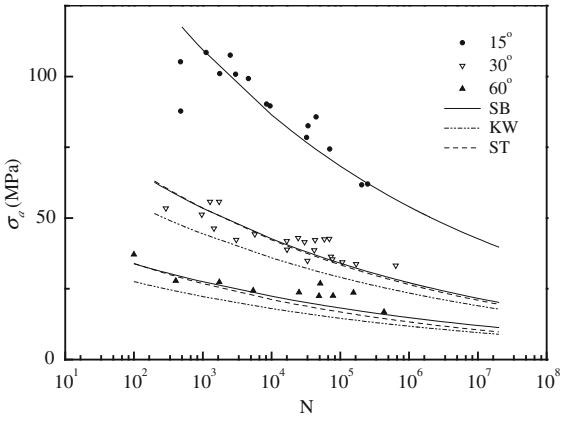

Fig. 6.13 Predicted S–N curves for 15°, 30° and 60° off-axis specimens [8], SB, KW and ST criteria

FTPF and SB predictions are similar since for this case, where the compressive strengths are considered equal to the tensile strengths, the only difference between the Tsai-Hill and Tsai-Hahn criteria, on which the two fatigue theories were founded, is the interaction term ($1/X^2$ for Tsai-Hill and $1/XY$ for Tsai-Hahn), which does not greatly affect the predictions compared with the rest of the terms of the failure tensor polynomial.

The 15° off-axis S–N curve has been arbitrarily selected as the reference one for the application of the FWE, KW and ST criteria. However, as also reported elsewhere, e.g., [16, 20, 30], criteria based on this "master" curve concept (like FWE, KW and ST) are quite sensitive to the selection of the reference curve. A comparison of the theoretical predictions of the FWE criterion to the 30° off-axis fatigue data, using different reference curves, is presented in Fig. 6.14. As shown, selection of the S–N curve at 15° off-axis seems to produce the most accurate theoretical results, while the rest of the estimated S–N curves are conservative (ref. 5° and 20°) or highly non-conservative, especially for the low-cycle fatigue region (ref. 60°).

Table 6.9 Analytical comparison of fatigue failure theory predictions with experimental data

Off-axis angle	FTPF, σ_a	HR, σ_a	FEW, σ_a	SB, σ_a	KW, σ_a	ST, σ_a
5°	$639.96\ N^{-0.1019}$	$666.16\ N^{-0.1031}$	$740.96\ N^{-0.1251}$	$666.48\ N^{-0.1031}$	$459.93\ N^{-0.0921}$	$638.36\ N^{-0.1017}$
10°	$332.95\ N^{-0.1027}$	$331.15\ N^{-0.1026}$	$346.74\ N^{-0.1107}$	$331.29\ N^{-0.1027}$	$257.66\ N^{-0.0921}$	$331.65\ N^{-0.1017}$
15°	$221.64\ N^{-0.1022}$	$221.64\ N^{-0.1022}$	$221.64\ N^{-0.1022}$	$221.64\ N^{-0.1022}$	$221.31\ N^{-0.0921}$	$221.31\ N^{-0.1017}$
20°	$164.54\ N^{-0.1011}$	$162.14\ N^{-0.1008}$	$160.16\ N^{-0.0961}$	$162.22\ N^{-0.1008}$	$128.12\ N^{-0.0921}$	$164.93\ N^{-0.1017}$
30°	$106.58\ N^{-0.0980}$	$105.23\ N^{-0.0981}$	$100.85\ N^{-0.0873}$	$105.26\ N^{-0.0981}$	$83.91\ N^{-0.0921}$	$108.02\ N^{-0.1017}$
60°	$51.25\ N^{-0.0896}$	$51.07\ N^{-0.0896}$	$47.57\ N^{-0.0731}$	$51.08\ N^{-0.0896}$	$42.09\ N^{-0.0921}$	$54.20\ N^{-0.1017}$

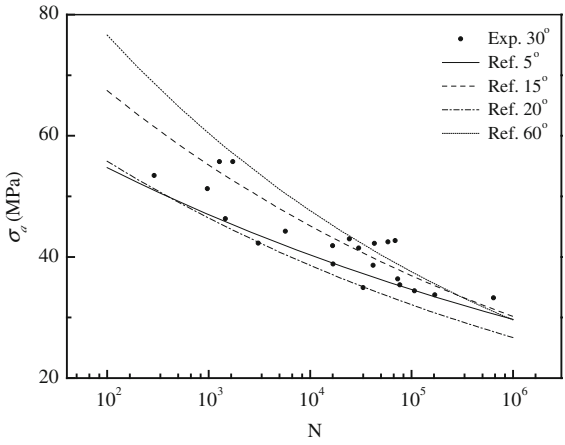

Fig. 6.14 Sensitivity of FWE criterion to reference curve

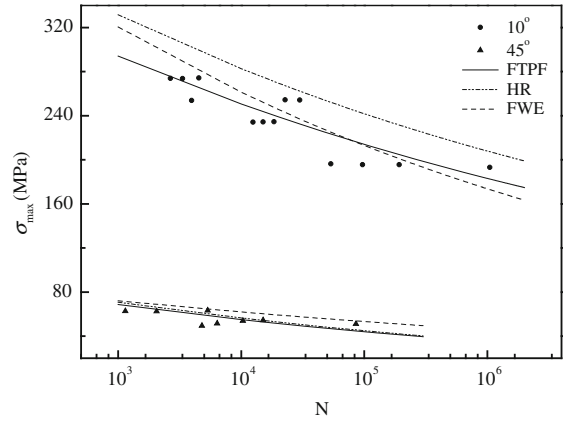

Fig. 6.15 Predicted S–N curves for 10° and 45° off-axis specimens [23], FTPF, HR and FWE criteria

6.4.1.2 Graphite/Epoxy, UD, Flat Specimens (Awerbuch and Hahn)

The results of the application of all the examined theories on the fatigue data of the material presented by Awerbuch and Hahn in [24] are presented in Figs. 6.15 and 6.16. The S–N curve at 20° off-axis was used as the reference curve for all the examined fatigue theories, when necessary, and the S–N curves at 10° and 45° were used for the evaluation of their predictive accuracy. The fatigue shear strength necessary for application of the FTPF and SB criteria was estimated by fitting the 20° off-axis fatigue data to Eq. 6.17, while the same dataset (the 20° off-axis S–N plus the S–N under the transverse direction) was used together with the corresponding static strength data, using Eq. 6.3 for estimation of the fatigue shear strength based on the HR criterion.

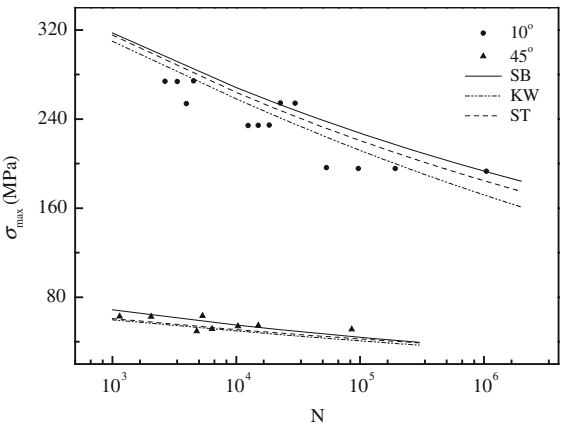

Fig. 6.16 Predicted S–N curves for 10° and 45° off-axis specimens [23], SB, KW and ST criteria

Table 6.10 Analytical comparison of fatigue failure theory predictions

Off-axis angle	FTPF, σ_{max}	HR, σ_{max}	FEW, σ_{max}	SB, σ_{max}	KW, σ_{max}	ST, σ_{max}
10°	$464.74\ N^{-0.0674}$	$509.98\ N^{-0.0649}$	$591.30\ N^{-0.0887}$	$508.53\ N^{-0.0700}$	$608.98\ N^{-0.0917}$	$538.60\ N^{-0.0775}$
45°	$136.66\ N^{-0.0984}$	$142.93\ N^{-0.1004}$	$113.60\ N^{-0.0658}$	$136.84\ N^{-0.0985}$	$117.36\ N^{-0.0917}$	$103.88\ N^{-0.0775}$

The predicted S–N curves of the examined material at 10° and 45° off-axis are presented in Fig. 6.15 for the FTPF, HR and FWE and in Fig. 6.16 for the SB, KW and ST criteria.

The predictions of the FTPF are the most accurate and consistent compared to those of the HR and FWE criteria. HR overestimates the behavior at 10° while it is accurate at 45°. The contrary applies to the FWE criterion for which the predicted S–N curve for 10° off-axis is corroborated well by the experimental data, being steeper however than the curve predicted from the FTPF. For the 45° off-axis specimens, the FWE criterion gives an optimistic prediction of the fatigue life.

In general, the predictions given by the examined theories are corroborated well by the experimental data, for both the small off-axis angle, 10°, and the 45°. However, KW and ST seem to be more conservative than SB for both the examined cases.

The estimated S–N curves in the form of the Log-Log curve are given in Table 6.10.

6.4.1.3 AS4 Carbon/PEEK APC2, Flat Specimens (Jen-Lee)

The material data from [13 and 14] were used for the evaluation of the predictive ability of the examined fatigue theories and detailed investigation of the influence of the reference curve selection on the accuracy of the fatigue theories that follow

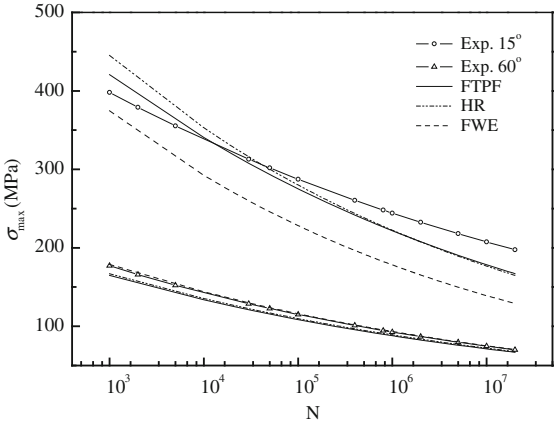

Fig. 6.17 Predicted S–N curves for 15° and 60° off-axis specimens under $R = 5$, FTPF, HR and FWE criteria. Ref. 45°

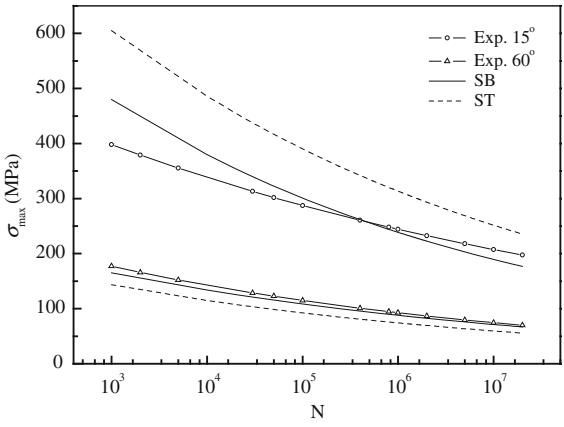

Fig. 6.18 Predicted S–N curves for 15° and 60° off-axis specimens under $R = 5$, SB, KW and ST criteria. Ref. 45°

the "master curve" concept, e.g., FWE, KW and ST. The FWE criterion will be used for the demonstration. The abundance of experimental data in the database of Jen and Lee [13, 14] allows the examination of the sensitivity of the polynomial-based fatigue failure criteria predictions on the off-axis angle also used for derivation of the material's shear fatigue strength. The FTPF criterion, which was proved more accurate than HR and SB for the previously examined fatigue datasets, will be used as a representative of this type of theory for the comparisons to the "master curve"-based theories.

The theoretical predictions are presented in Figs. 6.17 and 6.18 for the loading case of compression-compression under $R = 5$. The KW criterion cannot be applied in this case since non-negative stresses are present. The S–N curve at 45° was selected as the common reference for all the employed criteria for consistency. The experimental fatigue data at 15° and 60° off-axis angles were used for the comparisons. As presented in Figs. 6.17 and 6.18, the polynomial-based fatigue

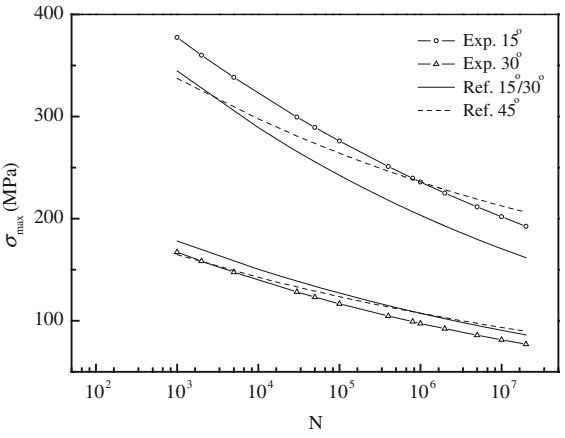

Fig. 6.19 Predicted S–N curves from FTPF for 15°, and 30° off-axis specimens [13, 14], $R = 0$. Different off-axis angles were used as the reference for the estimation of the shear fatigue strength

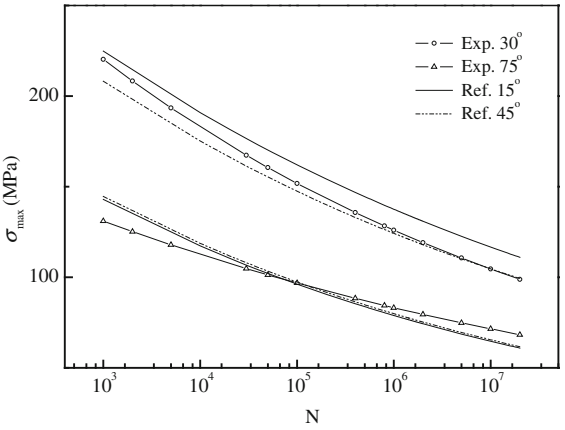

Fig. 6.20 Predicted S–N curves from FTPF for 30° and 75° off-axis specimens [13, 14], $R = -\infty$. Different off-axis angles were used as reference for estimation of shear fatigue strength

failure theories produce more accurate theoretical predictions than those based on the "master curve" concept. The FWE criterion is conservative, as presented in Fig. 6.17, while the ST criterion is conservative for the off-axis angle of 60°, but becomes highly non-conservative for the off-axis angle of 15°, see Fig. 6.18.

An assessment of the sensitivity of the examined fatigue theories has also been made in this section. FTPF and FWE were selected and applied for estimation of the off-axis fatigue life of the examined material, using different reference curves. The theoretical predictions of FTPF for specimens cut at the off-axis angles of 15° and 30° and tested under tension-tension loading, at $R = 0$, are presented in Fig. 6.19, together with the fitted curve to the experimental data. Two predicted curves are shown for each case, corresponding to two different reference curves. A similar process was followed ($R = -\infty$) and different off-axis angles (30° and 75°) and the results are presented in Fig. 6.20.

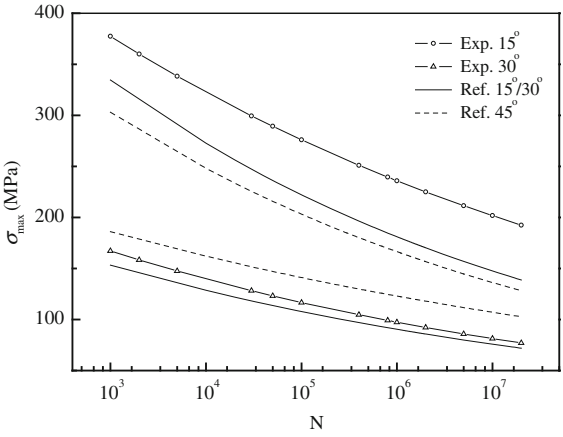

Fig. 6.21 Predicted S–N curves from FWE for 15° and 30° off-axis specimens [13, 14], $R = 0$. Different off-axis angles were used as reference for estimation of shear fatigue strength

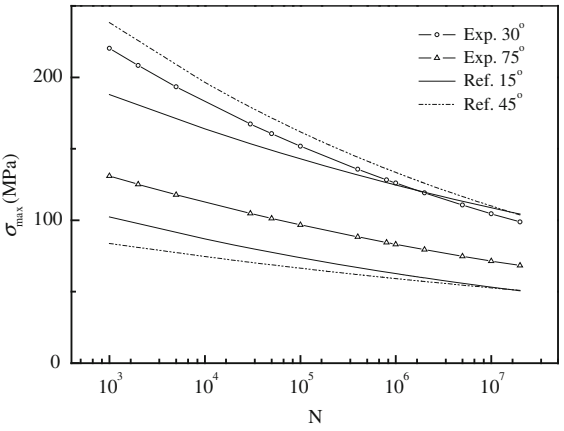

Fig. 6.22 Predicted S–N curves from FWE for 30° and 75° off-axis specimens [13, 14], $R = -\infty$. Different off-axis angles were used as reference for estimation of shear fatigue strength

Observation of Figs. 6.19 and 6.20 leads to the conclusion that the FTPF fatigue theory is relatively insensitive to the selection of the reference curve used for derivation of the shear fatigue strength of the material by means of Eq. 6.18 and is able to simulate the fatigue behavior of the examined material with acceptable accuracy. All the estimated S–N curves lie on a narrow band on the S–N plane with differences between them, and between them and the experimental data, of less than one decade of life, which is in a lot of cases the typical scatter of the experimental results for composite laminates.

The same process was followed for the FWE criterion and the results are presented in Figs. 6.21 and 6.22. FWE is shown to be quite sensitive to the selection of the reference curve as it can produce accurate, conservative or non-conservative theoretical predictions for different choices. Independent of the accuracy of the theoretical predictions of the FWE criterion, the presented scatter is very large, in some of the examined cases reaching even three to four decades of

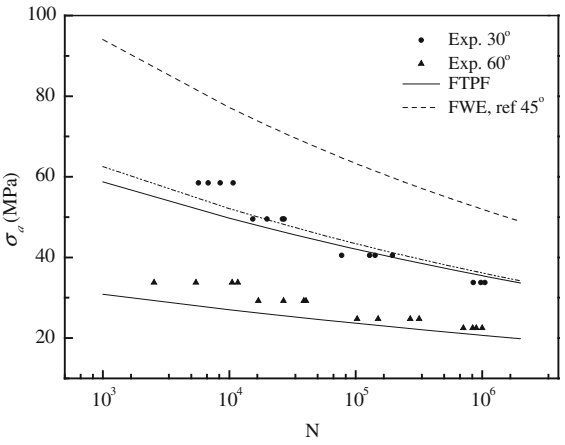

Fig. 6.23 Predicted S–N curves from FTPF and FWE for 30° and 60° off-axis specimens, $R = 10$

life (see Fig. 6.22, e.g., $\sigma_{max} = 100$ MPa, estimated N equals ca. 10^3, when the S–N at 15° is used as the reference, while the actual value is ca. 10^5).

6.4.1.4 Glass/Polyester, Multidirectional, Flat Specimens (Chap. 2)

The comparison of the predictions of the off-axis fatigue behavior of the multidirectional composite laminate presented in Chap. 2 is made in this paragraph. Since this material is not unidirectional and moreover negative mean cyclic stresses were applied on the specimens, the KW and ST criteria cannot be applied. In addition, a mixed mode was observed during the failure of the examined specimens and therefore the use of the HR fatigue theory is also excluded. From the remaining criteria–FTPF, FWE and SB–the first two will be employed in the following as representative of the polynomial-based theories (FTPF) and theories based on the master curve concept (FWE).

Calculations based on the two examined fatigue theories were performed using the material data presented in Chap. 2. Estimation of the fatigue life of specimens cut at different off-axis angles and loaded under different stress ratios was possible. For the application of the FTPF criterion on this dataset, it had previously been proved [17] that the derivation of the shear fatigue strength based on the experimentally derived curve for 45° off-axis was appropriate. The shear fatigue strength for S–N formulations were derived by dividing the corresponding S–N curves at 45° by a factor of 2.2 [17]. The S–N curves at 45° were also used as the reference curves for the application of the FWE criterion.

The results, presented in Figs. 6.23, 6.24 and 6.25, indicate a superior predictive ability of the FTPF criterion compared to the FWE. In all cases but one ($R = 0.1$, 15° off-axis, Fig. 6.25) FTPF's predictions are accurate and on the safe side, i.e., the predicted S–N curves are conservative when compared to the experimental data. On the other hand, the predictions produced by application of

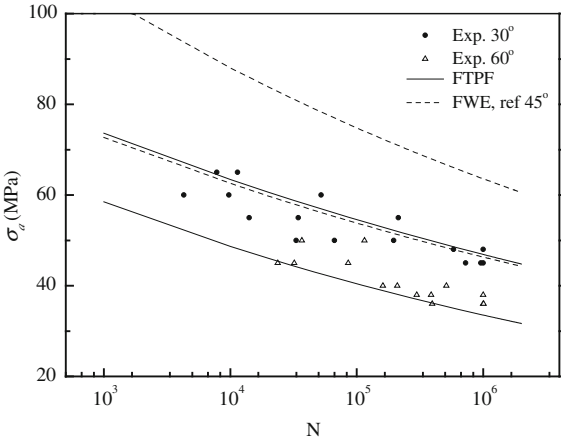

Fig. 6.24 Predicted S–N curves from FTPF and FWE for 30° and 60° off-axis specimens, $R = -1$

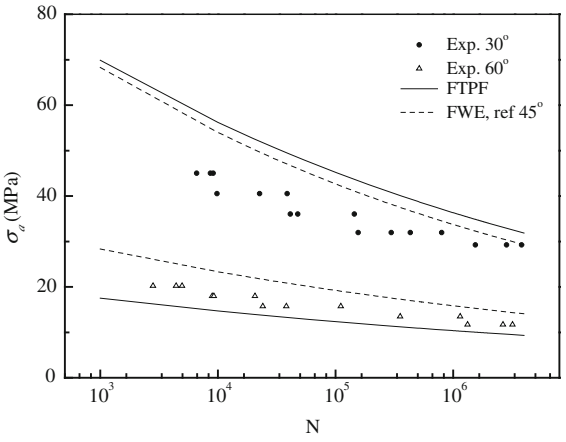

Fig. 6.25 Predicted S–N curves from FTPF and FWE for 15° and 75° off-axis specimens, $R = 0.1$

the FWE criterion are mainly non-conservative, estimating a longer fatigue life than that experimentally determined for all the examined cases. The difference between the theoretical and actual lifetime ranges between half (as it is also the average scatter of the available experimental data) and three decades of life, as for example presented in Fig. 6.23 for the 60° off-axis angle.

It should be mentioned however that FWE criterion can be more accurate if an S–N along a different on- or off-axis angle will be employed as the reference curve. The selection, for example, of the on-axis S–N curve as the reference for the loading case of $R = 10$ is proved more appropriate than the 45° off-axis, as presented in Fig. 6.26, where the predictions of the FWE criterion of the 30° and 60° off-axis angles are compared to the experimental data. The examined fatigue theory can even be more accurate, see for example Fig. 6.27, where the predictions of the fatigue life of the on-axis and 60° off-axis specimens fatigued under

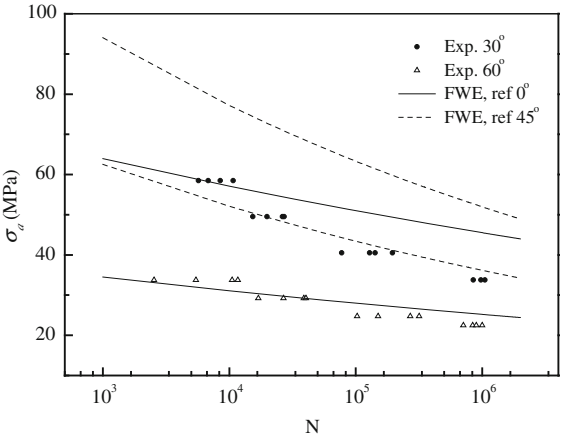

Fig. 6.26 Predicted S–N curves from FWE for 30° and 60° off-axis specimens, $R = 10$, based on different reference curves

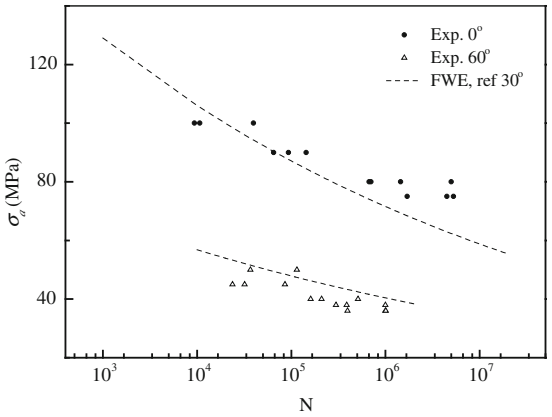

Fig. 6.27 Predicted S–N curves from FWE for 0°, and 60° off-axis specimens, $R = -1$, ref. 30°

reversed loading are presented. The S–N curve of the specimen cut at 30° off-axis has been used as the reference for the application of the FWE criterion and very accurate results were obtained. Although these very good predictions strengthened the validity of the FWE criterion, it also proved its main disadvantage: it is very sensitive to the selection of the reference angle and its results can be accurate or not according to a successful or unsuccessful decision concerning the selection of the reference curve.

6.4.2 Biaxial Loading

Biaxial fatigue data from the literature will also be employed for evaluation of the predictive ability of the aforementioned fatigue theories. The available biaxial fatigue data refer to woven cylindrical specimens either loaded under biaxial plane

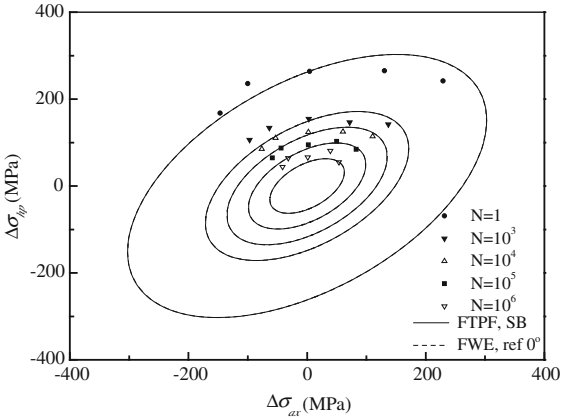

Fig. 6.28 Comparison of theoretical (predicted by FTPF, SB and FWE) failure loci vs. experimental data of cylindrical specimens loaded at 0°. FWE, ref. 0°

stress state comprising axial and tangential normal stresses, Owen and Griffiths [10], or biaxial plane stress states comprising axial normal and torsional (shear) stress components as presented by Fujii and Lin [11].

Only three of the examined fatigue theories are applicable to the material used in these studies, the FTPF, SB and FWE, while the rest cannot be applied for different reasons. HR is not applicable since for the woven material it is not possible to separate the failure modes into fiber- or matrix-dominated. On the other hand, KW and ST are applicable only for unidirectional composite laminates.

6.4.2.1 Biaxial Loading of Thin-Walled Tubes

Owen and Griffiths [10] examined glass/polyester thin-walled tubes under combined axial loading and internal pressure under the stress ratio of $R = 0$. Additionally, laminates of the same material were tested at fiber directions of 0° and 45° to estimate the axial and shear fatigue strength of the examined material. The longitudinal and transverse static strengths were $X = Y = 262.2$ MPa, while shear strength was $S = 110$ MPa. The shear fatigue strength was estimated based on the FTPF criterion Eq. 6.18 using the S–N curve at 45°. Both S–N curves from the specimens loaded at 0° and 45° were used as reference for application of the FWE criterion.

The fatigue theories were applied and the predicted failure loci are shown in Figs. 6.28, 6.29, 6.30 and 6.31 for the cylindrical specimens of [10] loaded at 0° and 45°, respectively.

As presented in Figs. 6.28, 6.29, 6.30 and 6.31, the FTPF and SB coincide since the examined woven material exhibits equal strength in the longitudinal and transverse directions, and they generally produce acceptable predictions. The FWE criterion also leads to accurate theoretical predictions, similar to the predictions of the previous two criteria.

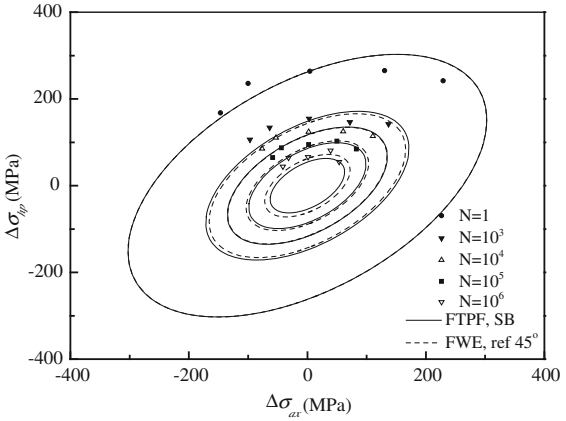

Fig. 6.29 Comparison of theoretical (predicted by FTPF, SB and FWE) failure loci vs. experimental data of cylindrical specimens loaded at 0°. FWE, ref. 45°

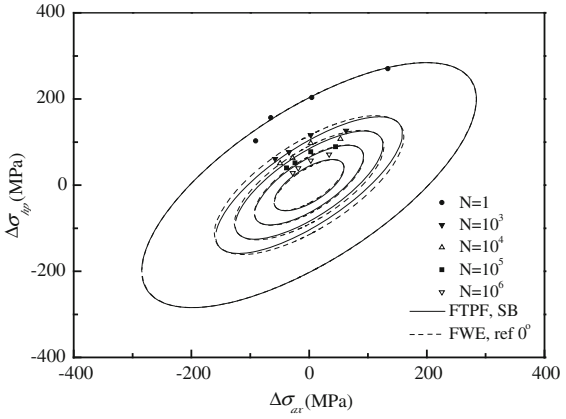

Fig. 6.30 Comparison of theoretical (predicted by FTPF, SB and FWE) failure loci vs. experimental data of cylindrical specimens loaded at 45°. FWE, ref. 0°

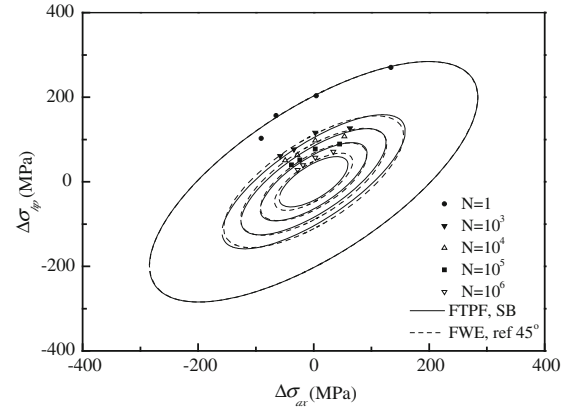

Fig. 6.31 Comparison of theoretical (predicted by FTPF, SB and FWE) failure loci vs. experimental data of cylindrical specimens loaded at 45°. FWE, ref. 45°

This occurs because all the examined theories result in similar relationships for the estimation of the failure loci for each loading condition. For the woven material of [10] loaded by an on-axis biaxial plane stress field comprising the normal stress components σ_1 and σ_2, the failure locus for each biaxial ratio, $a_1 = \sigma_1/\sigma_2$, can be estimated by:

$$\sigma_x^{FTPF} = \pm\frac{X(R,N,\theta)}{\sqrt{1+\alpha_1^2-\alpha_1}} \tag{6.29}$$

When the FTPF or SB criterion is used, while for the FWE the relationship becomes:

$$\sigma_x^{FWE} = \pm\frac{X}{X_r}\frac{X(R,N,\theta)}{\sqrt{1+\alpha_1^2-\alpha_1}} \tag{6.30}$$

with X denoting the static strength along the axial (longitudinal) direction, and $X(R, N, \theta)$ denoting the corresponding S–N curve, as a function of the fatigue stress ratio, R, number of cycles, N and angle, θ. The subscript r designates the reference angle.

According to Eqs. 6.29 and 6.30, when the on-axis direction is used as the reference, since the ratio $X/X_r = 1$, and $X(R, N, \theta) = X_r(R, N, \theta)$, the predictions of all criteria must coincide, as proved in Fig. 6.28. The differences between the FTPF or SB and FWE predictions seen in Fig. 6.29 are due to the use of the S–N curve of the 45° specimen. However, for the examined material the use of this reference has little influence on the results (the S–N curve of the on-axis specimens can accurately be predicted from the S–N at 45° and the FWE criterion). Therefore, the differences presented in Fig. 6.29 are not significant.

For the derivation of the failure loci at 45° for the same plane stress field, Eqs. 6.29 and 6.30 become:

$$\sigma_x^{FTPF} = \pm\frac{2X(R,N,\theta)}{\sqrt{(1+\alpha_1)^2+\left(\frac{X(R,N,\theta)}{S(R,N,\theta)}\right)^2(\alpha_1-1)^2}} \tag{6.31}$$

$$\sigma_x^{FWE} = \pm\frac{X}{X_r}\frac{2X(R,N,\theta)}{\sqrt{(1+\alpha_1)^2+\left(\frac{X}{S}\right)^2(\alpha_1-1)^2}} \tag{6.32}$$

with S and $S(R, N, \theta)$ denoting the shear static and fatigue strengths, respectively.

In this case, the similarity of the predictions, in addition to the effect of the reference curve selection, are also affected by the resemblance of the ratio between X and S when compared to the ratio $X(R, N, \theta)/S(R, N, \theta)$. The aforementioned ratios are given in Table 6.11 for different numbers of cycles between 1,000 and 1,000,000.

As shown in Table 6.11, the ratio between the axial strength and the shear strength (considered as the reference for application of the FWE criterion) is

Table 6.11 Calculated difference between static and fatigue strength ratios (X/S) of woven material presented in [10]

N	A = X/S (262.2 MPa/ 110 MPa)	B = $X(R,N,\theta)/S(R,N,\theta)$ 416.74 $N^{-0.139}$/ 142.52 $N^{-0.1169}$	Difference % (A−B/A) 100
1,000	2.38	2.51	5.47
10,000	2.38	2.39	0.23
100,000	2.38	2.28	−4.74
1,000,000	2.38	2.15	−9.47

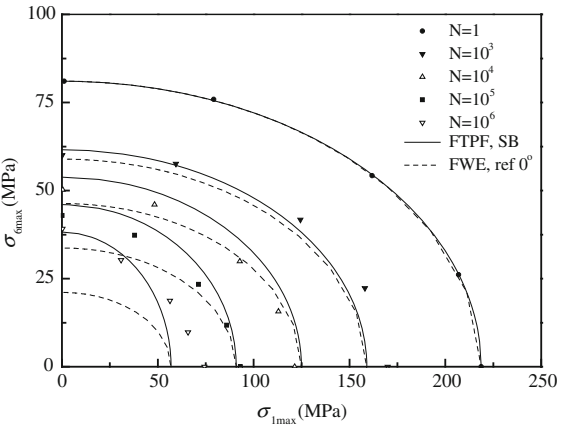

Fig. 6.32 Comparison of theoretical (predicted by FTPF, SB and FWE) failure loci vs. experimental data of cylindrical specimens loaded at 0°. FWE, ref. 0°

similar to the ratio between the corresponding fatigue strengths for different number of cycles. However, the static strength ratio is observed to be lower than the corresponding fatigue strength ratio for low number of cycles, $<10^5$, while this trend is reversed for number of cycles higher than 10^5. This behavior is also illustrated in Figs. 6.30 and 6.31. For $N = 10^5$ the predicted failure loci almost coincide, while they present differences for lower and higher numbers of fatigue cycles.

6.4.2.2 Biaxial Tensile-Shear Loading of Thin-Walled Tubes [11]

Woven glass/polyester tubes were examined by Fujii and Lin [11] under tensile and shear (torsion) loading under $R = 0$. The authors collected data under five biaxial ratios ($\alpha = \sigma_1/\sigma_6$), 1/0, 7/1, 3/1 1/1 and 0/1. The longitudinal and transverse normal strengths were $X = Y = 218.74$ MPa, while the shear strength was $S = 81.04$ MPa.

FTPF, SB and FWE were applicable for the examined case. As for the previously examined material, FTPF and SB predictions coincide. However, the FWE criterion proved very sensitive to the selection of the reference curve. As shown in Figs. 6.32 and 6.33, the criterion proved very conservative when the S–N curve

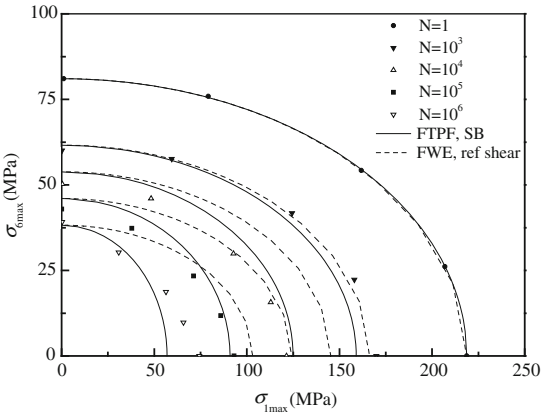

Fig. 6.33 Comparison of theoretical (predicted by FTPF, SB and FWE) failure loci vs. experimental data of cylindrical specimens loaded at 0°. FWE, ref. shear

under the biaxial ratio 1/0 (tensile loading) is used as the reference, see Fig. 6.32, but non-conservative when the S–N under shear loading was used as reference, Fig. 6.33.

For the present plane stress state that consists of normal and shear stress components, the failure loci for the two classes of examined criteria for any biaxial stress ratio, $a_2 = \sigma_6/\sigma_1$ can be derived by the following equations:

$$\sigma_{xa_2}^{FTPF} = \pm \frac{X(R,N,\theta)}{\sqrt{1 + \left(\frac{X(R,N,\theta)}{S(R,N,\theta)}\right)^2 \alpha_2^2}} \tag{6.33}$$

for the FTPF and SB criteria, and:

$$\sigma_{xa_2}^{FWE} = \pm \frac{X}{S} \frac{S(R,N,\theta)}{\sqrt{1 + \left(\frac{X}{S}\right)^2 \alpha_2^2}} \tag{6.34}$$

when the shear S–N curve is used as reference, while the corresponding equation for the reference based on the on-axis direction data becomes:

$$\sigma_{xa_2}^{FWE} = \pm \frac{X(R,N,\theta)}{\sqrt{1 + \left(\frac{X}{S}\right)^2 \alpha_2^2}} \tag{6.35}$$

The differences between the ratio of the static strengths and the corresponding ratio of the fatigue strengths are tabulated in Table 6.12 for different number of cycles between 1,000 and 1,000,000.

As shown, the difference between the two ratios increases with the number of cycles. Therefore, as also observed in Figs. 6.32 and 6.33, the predictions of the three criteria are similar for 1,000 cycles, while they become significantly different as the fatigue life is increased, with FWE criterion being less accurate for both cases of the selected reference angle. When the on-axis data is used as reference,

Table 6.12 Calculated difference between static and fatigue strength ratios (X/S) of woven material presented in [11]

N	A = X/S (218.74 MPa/ 81.32 MPa)	B = $X(R,N,\theta)/S(R,N,\theta)$ 405.65 $N^{-0.1309}$/ 97.05 $N^{-0.0649}$	Difference % (A−B/A) 100
1,000	2.69	2.65	−1.50
10,000	2.69	2.28	−15.39
100,000	2.69	1.96	−27.32
1,000,000	2.69	1.68	−37.57

FWE predicts material behavior accurately when $a_2 = 0$, while the predictions deviate significantly from the experimental data as the biaxial stress ratio increases, see Fig. 6.32. On the other hand, when the experimental data under shear loading are used as reference, the FWE criterion predicts well the behavior of the material for $a_2 = 1$, but deviates significantly from the actual material behavior for all the other cases. This observation confirms the aforementioned comments regarding the sensitivity of the FWE criterion for the selection of the reference data.

6.5 Evaluation of the Fatigue Theories

The following criteria were considered in order to evaluate the applicability of the examined fatigue theories and assess their influence on fatigue life prediction for the examined composite materials:

- Accuracy of predictions: quantified by the accuracy of predicting new S–N curves for off-axis angles or under biaxial loading patterns.
- Need for experimental data: quantified by the number of S–N curves required for the derivation of each model's parameters.
- Implemented assumptions and sensitivity to the data selected for modeling in relation to the consistency of the predictions: qualitative criterion.

The comparison of the results for unidirectional materials [8, 13, 14, 24] shows that the polynomial fatigue failure criteria give similar predictions with reasonable accuracy. On the other hand, predictions involving criteria based on the use of a "master curve" proved to be very dependent on the selection of the appropriate reference curve. It was proved that in most of the examined cases these criteria were significantly conservative or non-conservative compared to existing experimental results.

Only three of the examined fatigue theories (FTPF, SB and FWE) were applicable for the estimation of the fatigue life of the woven material tested under biaxial fatigue loading patterns. The results showed that the FTPF and SB criteria can be very accurate in this case, while the accuracy of the FWE criterion depends on the material. If the material off-axis fatigue behavior correlates well with the

corresponding static behavior (e.g. $X/S \approx X(R, N, \theta)/S(R, N, \theta)$), life predictions can be accurate.

Regarding the need for experimental data for estimation of the model parameters, it is obvious that theories based on a reference curve and static strength data are superior to the other examined criteria. However these theories comprise a number of assumptions, e.g. combining of static and fatigue data. The use of quasi-static strength data for the derivation of fatigue curves (such as fatigue data for 1 or ¼ cycle) is also arguable. No complete study on this subject has been made. Previous publications, e.g. [31], showed that quasi-static data should not be a part of the S–N curve, especially when they have been acquired under strain rates much lower that those used in fatigue loading. The use of quasi-static data in the regression leads to incorrect slopes of the S–N curves in [31]. On the other hand, excluding quasi-static data improved the description of the fatigue data, but introduced errors in lifetime predictions when the low cycle regime is important, as for example for loading spectra with a few high-load cycles. Moreover, they are liable to be inconsistent since they cannot guarantee that the prediction will not be affected by the selected reference curve. This characteristic is obvious in the case of the FWE criterion. The selection of a different off-axis angle to serve as reference curve can lead to very accurate, but also highly inaccurate, predictions as it was proved here and in [16, 20].

With the exception of the polynomial failure criteria, all the other examined fatigue theories are based on a number of assumptions that hinder if not prohibit their application for certain types of materials (e.g. HR cannot be applied when the failure modes of the material cannot be discriminated between fiber and matrix failure) or for certain loading patterns, such as the KW that was established only for fatigue loading patterns that do not include non-negative mean stresses.

6.6 Fatigue Design Considerations

The aim of the introduction and validation of multiaxial fatigue strength criteria, e.g., FTPF, FWE, is their potential practical application in the design of composite structures subjected to multiaxial, variable amplitude in general, fatigue stress states.

A composite structure may be composed of various laminate configurations. The examination of a number of fatigue theories in this chapter showed that two options are available if a multiaxial fatigue strength criterion is to be used in the design process; i) basic S–N curves of each lamina, which can be considered as the building layer of each laminate, must be known experimentally and laminate failure is theoretically predicted by means of a ply-by-ply analysis, as was assumed by the SB, KW and ST criteria, or ii) each laminate is considered as a different homogeneous anisotropic material whose basic strength properties must be measured experimentally, as assumed by the FTPF, FEW and HR fatigue theories. Obviously, in the first case only a limited number of tests have to be

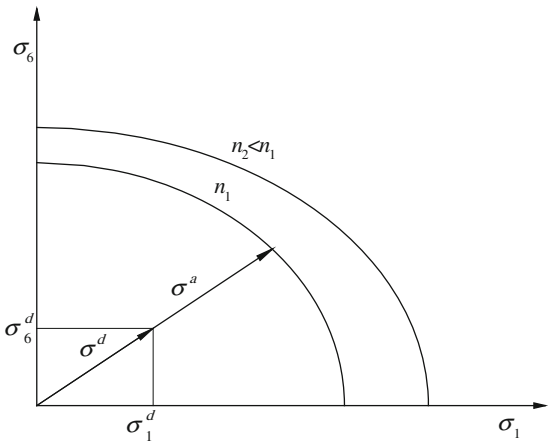

Fig. 6.34 Definition of strength ratio for fatigue

performed, but there is a lot of uncertainty regarding the remainder of the procedure, especially decisions concerning the degradation of ply properties after each ply failure.

If fatigue design is based on the second alternative, i.e., every multilayer configuration is considered to be a homogeneous anisotropic material with known basic S–N curves, and a polynomial-based fatigue failure criterion, e.g., FTPF, is used, the following comments apply.

6.6.1 Constant Amplitude Loading

In the special case where the developed stress fields are of constant amplitude, the dimensioning of the structure is a straightforward procedure. The strength ratio, *SR*, can be introduced for fatigue, having the same form as that for static loading [15]:

$$SR = \frac{\sigma_i^{\alpha}}{\sigma_i^d} \tag{6.36}$$

where σ_i^a is the allowable or ultimate cyclic stress for the number of cycles for which cyclic design stress σ_i^d is imposed on the structure. If the applied stress components for n_1 cycles are only normal, σ_i^d, and shear, σ_6^d, components for example, the correlation of σ_i^a and σ_i^d is shown in Fig. 6.34. The value of the strength ratio is given by the positive root of the following quadratic equation:

$$SR^2\left[F_{11}(n_1)\sigma_1^{d2} + F_{66}(n_1)\sigma_6^{d2}\right] + SRF_1(n_1)\sigma_1^d - 1 = 0 \tag{6.37}$$

In the above, it is assumed for simplicity that the stress ratio, $R = \sigma_{\min}/\sigma_{\max}$, of the design load is the same as that for which the basic S–N curves of the material are known. If material behavior must be theoretically simulated for different stress

ratios than those available after material characterization, constant life diagram formulations like those presented in Chap. 4 must also be employed.

6.6.2 Variable Amplitude Loading

In general, multiaxial fatigue loads imposed on a structure are time series of variable amplitude and mean value; the same is true for the respective developed stresses. Assuming that multiaxial stress time series of normal and shear stresses are proportional to each other, a simple rainflow counting method such as that introduced in [32] can be used to convert these variable amplitude stress time series into blocks of data of constant amplitude and mean values. The use of constant life diagrams—like those described in Chap. 4—allows the substitution of these stress values by equivalent stress amplitudes corresponding to a mean value equal to that assumed for the experimental determination of the basic S–N curves.

By following the above procedure, the pairs of σ_{1i} and σ_{6i} amplitudes for a certain number of operating cycles, n_{oi}, are determined. Using FTPF or any other reliable fatigue failure criterion, the number of cycles to failure, N_{fi}, under each pair of σ_{1i} and σ_{6i} can be calculated by solving Eq. 6.16 for N for example, and a multiaxial Miner coefficient can be introduced:

$$D = \sum_{i=1}^{k} \frac{n_{oi}}{N_{fi}} \tag{6.38}$$

where k is the total number of block loading patterns derived by the rainflow counting analysis.

6.7 Conclusions

The fatigue strength prediction of structures made of various composite material configurations operating under uniaxial or multiaxial loading conditions is the subject of this paper. The available failure criteria were examined and their predictive ability evaluated by the use of experimental data from the literature and the experimental program is presented in Chap. 2. These databases cover a wide range of GFRP and CFRP material configurations loaded under uniaxial and biaxial fatigue loads. The resulting complex stress fields are typical of those developed in the majority of engineering applications where composite materials are used.

The comparison between the evaluated criteria and the available experimental data showed that the polynomial fatigue failure criteria were very effective for estimation of the fatigue life of composite materials under complex fatigue stress states compared to those criteria based on one "master fatigue curve", which proved to be sensitive to the selection of this reference curve. However, considerably larger databases are necessary for the implementation of the polynomial criteria.

The accuracy of the examined multiaxial failure criteria in predicting the fatigue life of several composite material systems is generally acceptable. The application of the criteria proved to be easy and straightforward without the need for complicated numerical solutions. However, experience showed that the examined criteria can be accurate for one material and an examined loading case and highly inaccurate for another case. A commonly accepted complete fatigue theory does not yet exist, although some of the sub-problems have already been addressed.

The option to use laminate properties instead of lamina properties to predict laminate behavior enhances the applicability of the polynomial failure criteria (e.g. FTPF) for unidirectional and multidirectional lay-ups made up of any type of composite, e.g. unidirectional, woven or stitched layers. Especially under multiaxial loading, the polynomial failure theories (FTPF, SB) can produce acceptable fatigue failure loci for all the data considered, in contradiction with the FWE criterion, as used herein, which gives failure loci corroborated by the experimental multiaxial data only under certain conditions.

The efforts made with regard to fatigue failure prediction are aimed at more efficient design and consequently more accurate dimensioning of the parts of a structure. Using multiaxial strength criteria such as those described in this chapter, under constant amplitude loading, the lifetime is directly associated with the thickness of the laminate by using the fatigue strength ratio, *SR*. On the other hand, when the loading is irregular, a Miner coefficient for multiaxial stress states is introduced and the dimensioning is performed using an iterative procedure. The examined fatigue failure criteria can be used for investigation of the fatigue behavior of structural fiber-reinforced composite laminates under multiaxial stress states. Questions related to complex load proportionality, irregular stress spectra effects and potential validity of the constant life diagram formulations must be investigated before the proposed procedure can be used for realistic design cases.

References

1. Draft IEC 61400–1, Ed.2 (88/98/FDIS): 'Wind turbine generator systems–Part 1: Safety requirements', 1998
2. Germanischer Lloyd, 'Rules and regulations, IV–Non–marine technology', PART 1–WIND ENERGY, 1993
3. T.P. Philippidis, A.P. Vassilopoulos, Life prediction methodology for GFRP laminates under spectrum loading. Compos. Part A–Appl. Sci. **35**(6), 657–666 (2004)
4. J.A. Collins, *Failure of materials in mechanical design-analysis, prediction prevention.* (Wiley, New York, 1993)
5. R.F. Gibson, *Principles of Composite Material Mechanics* (McGraw-Hill Inc., New York, 1994)
6. O. Hoffman, The brittle strength of orthotropic materials. J. Compos. Mater. **1**(2), 200–206 (1967)
7. S.W. Tsai, E.M. Wu, A general theory of strength for anisotropic materials. J. Compos. Mater. **5**(1), 58–80 (1971)
8. Z. Hashin, A. Rotem, A fatigue failure criterion for fibre-reinforced materials. J. Compos. Mater. **7**, 448–464 (1973)

9. A. Rotem, Fatigue failure of multidirectional laminate. AIAA J. **17**(3), 271–277 (1979)
10. M.J. Owen, J.R. Griffiths, Evaluation of biaxial failure surfaces for a glass fabric reinforced polyester resin under static and fatigue loading. J. Mater. Sci. **13**(7), 1521–1537 (1978)
11. T. Fujii, F. Lin, Fatigue behavior of a plain-woven glass fabric laminate under tension/torsion biaxial loading. J. Compos. Mater. **29**(5), 573–590 (1995)
12. D.F. Sims,V.H. Brogdon, in *Fatigue Behavior of Composites under Different Loading Modes*, eds. by K.L. Reifsnider, K.N. Lauraitis. Fatigue of filamentary materials, (ASTM STP 636, 1977), pp. 185–205
13. M.-H.R. Jen, C.-H. Lee, Strength and life in thermoplastic composite laminates under static and fatigue loads. Part I: experimental. Int. J. Fatigue **20**(9), 605–615 (1998)
14. M.-H.R. Jen, C.-H. Lee, Strength and life in thermoplastic composite laminates under static and fatigue loads. Part II: Formulation. Int. J. Fatigue **20**(9), 617–629 (1998)
15. S.W. Tsai, H.T. Hahn, *Introduction to Composite Materials* (Technomic, Lancaster, 1980)
16. T.P. Philippidis, A.P. Vassilopoulos, Fatigue strength prediction under multiaxial stress. J. Compos. Mater. **33**(17), 1578–1599 (1999)
17. T.P. Philippidis, A.P. Vassilopoulos, Complex stress state effect on fatigue life of GRP laminates. Part II, Theoretical formulation. Int. J. Fatigue **24**(8), 825–830 (2002)
18. M. Kawai, A phenomenological model for off-axis fatigue behavior of unidirectional polymer matrix composites under different stress ratios. Compos. Part A-Appl. S **35**(7–8), 955–963 (2004)
19. Z. Fawaz, F. Ellyin, Fatigue failure model for fibre-reinforced materials under general loading conditions. J. Compos. Mater. **28**(15), 1432–1451 (1994)
20. M. Quaresimin, L. Susmel, R. Talerja, Fatigue behaviour and life assessment of composite laminates under multiaxial loadings. Int. J. Fatigue **32**(1), 2–16 (2009)
21. H. El Kadi, F. Ellyin, Effect of stress ratio on the fatigue failure of fiberglass reinforced epoxy laminae. Composites **25**(10), 917–924 (1994)
22. M.M. Shokrieh, F. Taheri-Behrooz, A unified fatigue life model for composite materials. Compos. Struct. **75**(1–4), 444–450 (2006)
23. R.S. Sandhu, R.L. Gallo, G.P. Sendeckyj, in *Initiation and Accumulation of Damage in Composite Laminates*, ed. by I.M. Daniel (ASTM STP 787, 1982), pp. 163–182
24. J. Awerbuch, H.T. Hahn, in *Fatigue of Fibrous Composite Materials*. ed. by K.N. Lauraitis. Off-axis fatigue of graphite/epoxy composites, (ASTM STP 723, 1981), pp. 243–273
25. S. Lee, M. Munro, Evaluation of in-plane shear test methods for advanced composite materials by the decision analysis technique. Composites **17**(1), 13–22 (1986)
26. S.W. Fowser, R.B. Pipes, D.W. Wilson, On the determination of laminate and lamina shear response by tension tests. Compos. Sci. Technol. **26**, 31–36 (1986)
27. A. Smits, D. Van Hemelrijck, T.P. Philippidis, A. Cardon, Design of a cruciform specimen for biaxial testing of fibre reinforced composite laminates. Compos. Sci. Technol. **66**(7–8), 964–975 (2006)
28. M.J. Hinton, A.S. Kaddour, P.D. Soden, *Failure Criteria in Fibre Reinforced Polymer Composites: The World-Wide Failure Exercise, a Composite Science and Technology Compendium* (Elsevier, Amsterdam, 2004)
29. T.P. Philippidis, P.S. Theocaris, Failure prediction of fibre reinforced laminates under hygrothermal and mechanical in-plane loads. Adv. Pol. Tech. **12**(3), 271–279 (1993)
30. A.P. Vassilopoulos, R. Sarfaraz, B.D. Manshadi, T. Keller, A computational tool for the life prediction of GFRP laminates under irregular complex stress states: Influence of the fatigue failure criterion. Comp. Mat. Sci. **49**(3), 483–491 (2010). 10.1016/j.commatsci.2010.05.039
31. R.P.L. Nijssen, O. Krause, T.P. Philippidis, Benchmark of lifetime prediction methodologies. Optimat Blades technical report, 2004, OB_TG1_R012 rev.001, http://www.wmc.eu/public_docs/10218_001.pdf
32. S.D. Downing, D.F. Socie, Simple rainflow algorithms. Int. J. Fatigue **4**(1), 31–40 (1982)